

UC Santa Cruz

UC Santa Cruz Electronic Theses and Dissertations

Title

Adapting Chirp Spread Spectrum Modulation Techniques for Visible Light Communication in Greenhouses

Permalink

<https://escholarship.org/uc/item/7cv1r6bw>

Author

Lin, Jack

Publication Date

2024

Copyright Information

This work is made available under the terms of a Creative Commons Attribution-NonCommercial License, available at <https://creativecommons.org/licenses/by-nc/4.0/>

Peer reviewed|Thesis/dissertation

UNIVERSITY OF CALIFORNIA
SANTA CRUZ

**ADAPTING CHIRP SPREAD SPECTRUM MODULATION
TECHNIQUES FOR VISIBLE LIGHT COMMUNICATION IN
GREENHOUSES**

A thesis submitted in partial satisfaction
of the requirements for the degree of

MASTER OF SCIENCE

in

ELECTRICAL AND COMPUTER ENGINEERING

by

Jack Lin

March 2025

The Thesis of Jack Lin
is approved:

Professor Colleen Josephson, Chair

Professor Katia Obraczka

Professor Michael Loik

Peter Biehl
Vice Provost and Dean of Graduate Studies

Copyright © by

Jack Lin

2025

Table of Contents

List of Figures	v
Abstract	viii
Acknowledgments	ix
1 Introduction	1
1.1 Problem Statement	1
1.2 Outline of Thesis	4
2 Background	5
2.1 Greenhouses and Greenhouse Technologies	5
2.2 Lighting	6
2.3 Argus Controls	8
2.4 Actuation and Sensing	11
2.5 RF-Based Wireless Communication	11
2.6 Visible Light Communication	13
2.6.1 On Off Keying	16
2.6.2 Chirp Spread Spectrum and LoRa	17
3 Design, Implementation, and Evaluation of FIAT LUX’s Downlink	18
3.1 Specific Background on VLC and CSS	18
3.2 VLC System Overview	24
3.3 Interfacing with the XtremeLUX LEDs	24
3.4 Experimental Methodology	27
3.4.1 Simulation	28
3.4.2 FIAT LUX Prototype	32
3.5 Experimental Results	36
3.5.1 FIAT LUX Prototype Results	36
3.5.2 Simulation Results	39
4 Greenhouse Integration	42
4.1 Traditional IoT System Overview	42
4.2 Design and Implementation	42

4.2.1	Argus Interface	45
4.3	Results	48
5	Discussion and Future Work	50
6	Conclusion	54
	Bibliography	56

List of Figures

2.1	The general photosynthetic response of plants to various wavelengths of visible light. The range between 400 nm and 700 nm is regarded as the photosynthetic active radiation (PAR) regime in which plants exhibit strong photosynthetic activity.	8
2.2	Block diagram depicting the commercial solution proposed by Argus Controls. In this diagram, a single Argus Omnisensor is reads the temperature and relative humidity close to the plant (in a device labeled with “IoT Tag”). The Argus Omnisensor communicates its sensor readings with the Argus Controls center’s Titan I/O Module for environmental control via the lights, fans, and more.	9
2.3	Panoramic interior view of the UCSC Coastal Science Campus greenhouse prior to LED renovations. The Argus infrastructure panels, 1000 W metal halide lamps, and the Argus Omnisensor are annotated.	10
2.4	Argus Omnisensor microcontroller board with annotations describing key components which connects to the sensor board (Figure 2.5) to perform sensor readings and pass sensor data upstream.	12
2.5	Argus Omnisensor sensor board which interfaces with the microcontroller board (Figure 2.4) to provide temperature and relative humidity sensing capabilities.	12
3.1	The proposed CSS frame adapted for optical communication.	19
3.2	Illustration of chirp detection in a noisy environment.	22
3.3	Novel VLC system diagram. Of this system, the communication downlink between the Sensor Manager and the IoT Tag was built and evaluated in FIAT LUX.	25
3.4	FIAT LUX’s architecture and functional components.	26
3.5	Time domain representation of three example chirp signals.	29
3.6	Spectrogram representation of the three example chirp signals shown in Figure 3.5.	29
3.7	Simulation workflow for modulation and demodulation of an OOK VLC signal. $r[n]$ represents the array of received samples, $r_{avr}[m]$ is the sliding window average, and $d[m]$ is the corresponding ‘0’ or ‘1’ obtained from the average being above or below the set threshold.	30

3.8	Simulation workflow for modulation and demodulation of a CSS VLC signal. sv represents the symbol value being evaluated, cs is the corresponding chirp for the selected symbol value, $d[n]$ is the received samples multiplied with the base down-chirp, $D[n]$ is the frequency content of the time-domain signal, and $D_filter[n]$ is the frequency content of that signal after applying a bandpass filter to remove unwanted low and high frequency noise.	31
3.9	Typical quantum efficiency of a PV cell. The PV cell's response to red and blue wavelengths is reduced, and is most active in the center of the 400 nm to 700 nm range. Image retrieved from [28].	32
3.10	FIAT LUX receiver, which consists of a BBB, an analog optical front-end, and the solar panels. Experimental setup to evaluate the performance of the FIAT LUX receiver at distance. The transmitter light bar LBRB9 is oriented such that it is perpendicular to the receiver. The receiver is located on the left and is situated mid-height to the light bar.	33
3.11	Fiat Lux receiver schematic.	34
3.12	Experimental setup for evaluating FIAT LUX's range and noise resilience which is aligned with Figure 3.4	35
3.13	Comparison of simulated CSS versus experimental CSS implementation with $SF = 8$ between 0 and 4 meters. In the CSS experiment, no ambient noise was added (i.e. dark room).	37
3.14	Simulation results which compare simulated OOK against simulated CSS at various distances and with $SF = 8$	39
3.15	Simulation results which compare simulated OOK against simulated CSS (with $SF = 7, 8, 12$) under various amounts of ambient light. The amount of ambient light added to the signal is expressed here in terms of SNR at the receiver. For reference, in FIAT LUX SNR indoors is approximately +10 dB, while the SNR outdoors is approximately -30 dB (at 1 meter with the LBRB9 LED and SM141K04LV solar panels).	41
4.1	System diagram for the traditional IoT deployment. The two main components developed in this chapter are the IoT Tag and the Sensor Manager.	43
4.2	Argus Isolated Device Network Board (ISODN). The ribbon cable connects the ISODN with the Argus control panel. The screw terminal connects the ISODN with the BBB via a USB to RS-485 cable. Image retrieved from [9].	46
4.3	Argus Titan Controller and Argus ISODN: Isolated (Optical) Device Network Board circled in red.	47

- 4.4 Argus Controls environmental status graph of a greenhouse equipped with a traditional IoT sensor that I designed. The short orange (traditional IoT) line below the magenta line (Argus Omnisensor) shows that the temperature tracks the Argus Omnisensor, but may need offset adjustment. (Note: the Omnisensor was suspended approximately 1.5 m above the ground in the center of the greenhouse, while the traditional IoT sensor tag was placed on a bench approximately 1 m above the ground at a corner of the greenhouse. The difference in observed temperature at the two sensor placement areas indicates the necessity for locationally-relevant sensor readings in greenhouses.) 49

Abstract

Adapting Chirp Spread Spectrum Modulation Techniques for Visible Light Communication in Greenhouses

by

Jack Lin

As greenhouses and other forms of protected agriculture modernize their systems and adopt data-driven techniques in reaction to climate change, wireless agricultural sensing is rapidly becoming an emergent area of research. Due to high energy and resource consumption in greenhouses, low-power systems capable of autonomous greenhouse control will be critical for next-gen greenhouses in order to help address food security and climate resilience. To fill this gap, I develop an ultra-low power wireless communication technique that can be utilized for precision agriculture in greenhouses. The proposed solution uses a chirp spread spectrum (CSS) based visible light communication (VLC) downlink that is capable communicating 2 meters using agricultural grow light light emitting diodes (LEDs). VLC coupled with the high noise resilience of CSS permits the transmission of data even under high irradiance conditions such as greenhouses, thereby enabling locationally-relevant sensor placement. In this thesis, in addition to describing the CSS VLC downlink, I also present performance results obtained through simulation experiments as well as experiments with the current CSS VLC prototype.

Acknowledgments

Without the support of my family, friends, and colleagues, this work would not have been possible. To my family, I am grateful for their unfailing love and acceptance. I am thankful to my advisor, Professor Colleen Josephson, for her guidance and mentorship during my time in her lab. Her support cannot be understated in its impacts on both the progress of the work described here and on my own personal growth. Likewise, I would also like to extend my gratitude to Professor Katia Obraczka and Professor Michael Loik not only for lending their knowledge in the development of the project, but also for their patience during the revision of this thesis. To my fellow collaborators Matt Kaltman, Yawen Guo, Firouz Vafadari, and Tyler Morton, I am appreciative of their expertise and efforts in bringing the project to fruition. I am thankful to the UCSC Greenhouse Manager Sylvie Childress for extending facilities and support for the deployment of the system. Lastly, I am very thankful to my colleagues and friends in the jLab for the camaraderie and fellowship both in and outside of the lab. Without the support of this capable and caring community, we would not have been able to achieve success. I cherish the time that we have spent together so far and look forward to what we can accomplish together in the future. Thank you!

Chapter 1

Introduction

1.1 Problem Statement

Protected agriculture such as greenhouses have become increasingly popular as a way to counteract the effects of climate change. In California alone, the number of protected agriculture operations increased by 20% between 2018 and 2023 [33] [35]. As for the U.S. at large, the square footage of crops grown under protection increased by 3.2% between 2017 and 2022 [34].

Greenhouses are a form of protected agriculture that insulates crops from their external environment. This allows greenhouses to provide a controlled environment for plants that would otherwise not flourish outside. These greenhouses can feature multiple climate control mechanisms, such as glass walls to trap heat and intensify light, swamp coolers to regulate temperature and humidity, lighting to prolong or intensify light, and more. These mechanisms allow for precise control over the plant growth environment, but they can require special tooling and equipment as well as additional resources to

manage and control.

Commercial solutions such as those provided by Argus Controls (headquartered in Langley, British Columbia, Canada) give greenhouse managers a turnkey solution for monitoring, scheduling, and controlling greenhouses. Here at UCSC, many of the instructional and research greenhouses are equipped with Argus infrastructure. While they provide greenhouse managers with a high degree of control over their greenhouses, one of the key limitations of Argus is that they rely on wired infrastructure, which limits the placement of sensors and thus the precision of the information that those sensors can gather. While greenhouse managers are hindered by the lack of locational precision of the Argus sensors, of even more importance is the minimization of the energy cost and carbon footprint of their greenhouses.

An increasing number of greenhouses are upgrading from traditional lighting to LED lighting in anticipation of upcoming minimum energy efficiency legislature for greenhouses [5], to reduce energy costs, and also to obtain finer control over the output light. Upgrading from traditional high intensity discharge (HID) lamps to LED lighting can result in more than 49% power savings while still achieving equivalent illuminance. For example, at the UCSC Coastal Science Greenhouses the old ParSource HID lamps consume 1000 W per lamp [27] while the new XtremeLux LF11 LED light fixtures consume 510 W per unit [41]. In addition to the cost savings, the LEDs also provide variable output control to dim the lights and adjustable output spectra to adapt the lighting to the type of crop. In contrast, the ParSource HID lamps are either on or off. The use of LEDs make it possible to implement a rapidly-developing form of wireless communications known as Visible Light Communication, or VLC for short. VLC is an

emerging alternative to traditional RF-based wireless protocols that avoids RF overcrowding issues that plague protocols such as WiFi. In device-dense areas such as greenhouses which may deploy multitudes of wireless sensors to monitor individual plant growth parameters, VLC may be more suitable than traditional wireless communication methods. My vision is that as greenhouses increasingly adopt LED lighting, those very same lights could be used not only to provide illumination to plants and power sensing devices, but also to host a visible light communication downlink. This VLC downlink connects to a diverse set of wireless sensor nodes which take advantage of the light for both communication and energy harvesting. For the uplink, I envision a low-power RF backscatter system to close the loop and send sensor data back upstream for analysis and greenhouse environmental control. RF backscatter is an attractive option because it consumes a fraction of the power when compared to traditional active wireless technologies like WiFi and LoRa, typically a few μW in backscatter versus hundreds of mW used in LoRa.

This thesis describes the work that I have done towards building my vision of a VLC downlink for greenhouses, enabling greenhouse sensing with higher locational precision and less energy consumption. The project is a multidisciplinary collaboration across multiple students and faculty advisors. This thesis describes the work that I personally undertook within the scope of the greater project. My contributions are as follows:

- Prototyping of a radio-frequency-based Internet of Things (IoT) solution similar to existing wireless solutions in order to provide a baseline for comparison and also

to understand how to integrate my VSS-based VLC downlink with the existing greenhouse system.

- Development of a noise-resilient chirp spread spectrum modulation scheme for visible light communication that will satisfy communication requirements in a noise-dense greenhouse environment. We name our CSS-based VLC system FIAT LUX.
- Evaluation of the FIAT LUX system through simulation and prototyping under a range of ambient noise scenarios to showcase the CSS-based VLC downlink noise immunity under different conditions.

1.2 Outline of Thesis

This thesis describes my CSS-based VLC downlink system and also discusses the work done on the greenhouses, both in preparation and in installation. I first discuss the background and prior work in more detail in Chapter 2 before describing the VLC work done for FIAT LUX in Chapter 3 and the greenhouse integration work in Chapter 4. Within the FIAT LUX and greenhouse integration work chapters, I discuss specific background, my experimental methodology to evaluate the performance of the proposed CSS-based VLC system, and the results. I provide a broader discussion of the results and areas for future work in Chapter 5 and end with a conclusion in Chapter (6).

Chapter 2

Background

2.1 Greenhouses and Greenhouse Technologies

Greenhouses have been used for hundreds of years as a way to protect and regulate plant growth [14]. The protected environment greenhouses provide allows plants to grow in otherwise hostile environments. Greenhouses come in many forms, and can have a variety of different construction materials, architectures, and use cases. Glasshouses are the most well-known example of greenhouses and are constructed of glass panes to permit light but trap heat and moisture. In this paper, I focus mostly on glasshouses as that is the type of greenhouse that is most commonly used at UCSC.

There are many challenges that greenhouse managers face. To list a few: upfront building costs, heating, air conditioning, water, electricity, chemicals, and labor all factor into the economic challenges of running a greenhouse. To reduce these barriers, many greenhouse technologies have been developed to address lacking capabilities or increase efficiency to reduce costs. For example, advanced construction materials allow

for selective light transmission and heat capture. Sensors provide a detailed view of greenhouse conditions and actuators provide the ability to change those conditions autonomously.

2.2 Lighting

Many greenhouses are equipped with additional lighting to supplement natural sunlight. For example, the greenhouses at the UCSC Coastal Science Campus use high intensity discharge (HID) lamps to extend the “daylight” hours in the greenhouse during the winter months. Besides high intensity discharge lamps, there are multiple kinds of lighting sources commonly in use at greenhouses. Some greenhouses use household incandescent bulbs which flow current through a filament to emit light, or fluorescent lights which flow current through a gas which glows. Larger scale greenhouse operations may opt to instead use higher power light sources such as metal halide or high pressure sodium lamps. These fall under the high intensity discharge category of lamps, which are similar to fluorescent lamps in that they both put a current through a gas to provide light. However, HID lamps include additional additives such as metal halide or sodium to adjust the color and intensity, and use a ballast tank to provide cooling to the high-power HID lights. More recently, LEDs have come into favor for use as grow lights in greenhouses due to their low power draw, high efficiency, and narrow emission band. LEDs emit photons at specific wavelengths depending on the band gap energy of the materials that the LED is constructed from. The emission spectra of a variety of lighting sources are discussed in [1].

In addition to the many types of lighting that are available, the quantification of light output also has many confusing metrics and units. To increase clarity, I will explain the meaning and relevance of several lighting metrics of interest.

For light sources, the most common unit for measuring output illuminance is the SI unit lumen (lm). A light source's lumens describes the total photon flow rate out of that light source, also called luminous flux (which is derived from the SI base units cd sr). This unit is often seen on common lightbulbs of all constructions (LED, incandescent, halogen, etc) as well as specialized lighting sources for plant growth (high pressure sodium, LED grow lights). One important caveat of lumens is that it describes the total photon output of all wavelengths, but it is weighted according to a human eye model via a "luminosity model". In this way, lumens is never a relevant metric to use when evaluating light sources for use in greenhouses for plant growth, since plants respond differently to wavelengths than humans.

Lux (lx) is a measure of the amount of luminous flux at a given location. In layman's terms, where lumens is putting a net around a lightbulb to catch all of its output rays, lux is holding a net flat on the ground to capture the luminous flux hitting a unit area. One lux is equal to one lumen per square meter ($\frac{\text{lm}}{\text{m}^2}$).

Where lumens and lux measure with respect to a human's perception to light, Photosynthetically Active Radiation (PAR) instead measures with respect to a plant's perception. For plants, the wavelengths of interest range between 400 nm to 700 nm. The output rate of photons within this range is photosynthetic photon flux (in units of $\frac{\mu\text{mol}}{\text{s}}$). Photosynthetic photon flux density (in units of $\frac{\mu\text{mol}}{\text{m}^2 \text{s}}$) is a measure of the photosynthetic photon flux per unit area. Figure 2.1 shows the typical photosynthetic

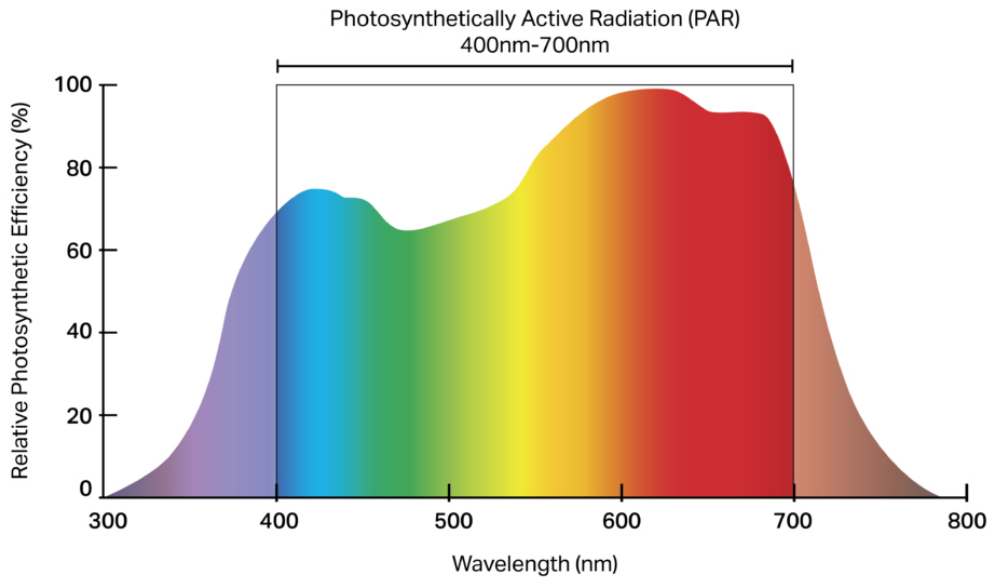


Figure 2.1: The general photosynthetic response of plants to various wavelengths of visible light. The range between 400 nm and 700 nm is regarded as the photosynthetic active radiation (PAR) regime in which plants exhibit strong photosynthetic activity. Image retrieved from [15].

response of plants, where the bulk of the sensitivity lies between 400 nm and 700 nm.

2.3 Argus Controls

Greenhouse monitoring and control is important for keeping a well-regulated environment for plant growth. One company that specializes in greenhouse control systems is Argus Controls. Argus provides a full end-to-end system which includes greenhouse sensors, actuators, networking, and scheduling/control. As shown in Figure 2.2, the Argus system relies heavily on a single Omnisensor to inform the actuators of when and how to regulate the greenhouse's environment.

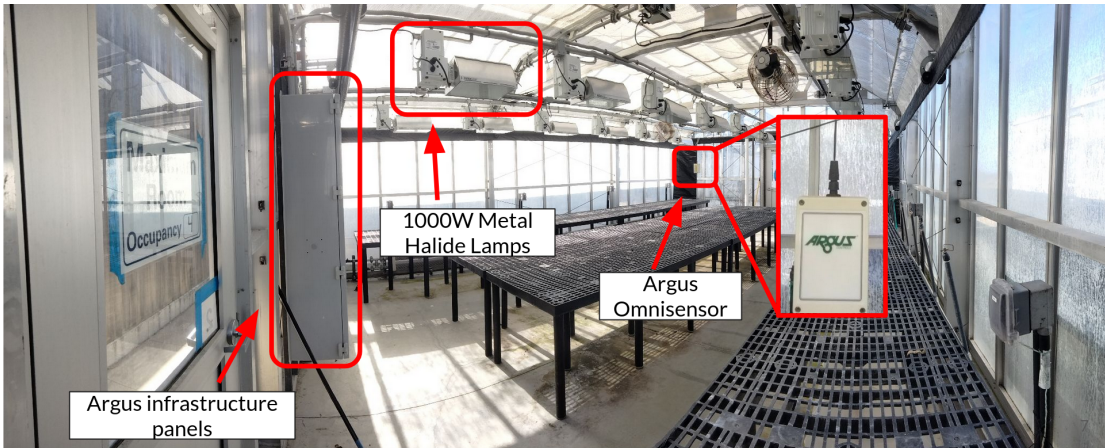


Figure 2.3: Panoramic interior view of the UCSC Coastal Science Campus greenhouse prior to LED renovations. The Argus infrastructure panels, 1000 W metal halide lamps, and the Argus Omnisensor are annotated.

At UCSC, Argus systems are deployed at all of the UCSC greenhouses, including the UCSC Coastal Science Campus greenhouses. They are equipped with eighteen 1000 W metal halide HID lamps and a single Argus Omnisensor suspended from the ceiling in the center of the greenhouse.

While Argus provides a complete turnkey solution, they also allow for external third party devices to be connected to the system. Third party devices are integrated into the Argus system at the Titan Control Access Point (TCAP) shown in Figure 4.3. At the Coastal Science Campus greenhouses, the master TCAP is located inside the greenhouse manager's office in the longhouse, and controls all six of the greenhouses there as well as the indoor grow chambers.

A separate module is required to allow third party devices to interface with the Argus ecosystem. This module is called the Isolated Optical Device Network (ISODN) board, depicted in Figure 4.3. The ISODN allows legacy Argus devices and third party

devices using the Modbus protocol (over RS-485) to connect to the Argus.

2.4 Actuation and Sensing

The Argus system deployed at the UCSC Coastal Science Campus greenhouses has a combination of sensors and actuators. To highlight some of the actuation features, the greenhouses have roof vents for ventilation, fans for circulation, swamp coolers for temperature and humidity regulation, perimeter heating for regulating temperature, shade curtains and blackout curtains for reducing light, and metal halide lamps for providing supplemental lighting.

For sensors, there is the all-in-one Argus Omnisensor (see Figures 2.4 and 2.5) suspended in the center of the room. The Omnisensor reads the temperature and relative humidity of the greenhouse. While more advanced versions of the Omnisensor carry CO₂ and Photosynthetic Active Radiation (PAR) detecting capabilities, the ones deployed at the UCSC Coastal Science Campus greenhouses only have temperature and humidity capabilities.

2.5 RF-Based Wireless Communication

One of the motivations for a wireless system is that it allows for higher precision sensing at locations of interest. For example, the temperature within the UCSC Coastal Science Greenhouse can vary by as much as 2 °C when measured in the center at canopy height (approximately 1.5 m) versus in the corner at bench-height (approximately 1 m). With a wireless system, more sensors could be placed within the greenhouse to obtain

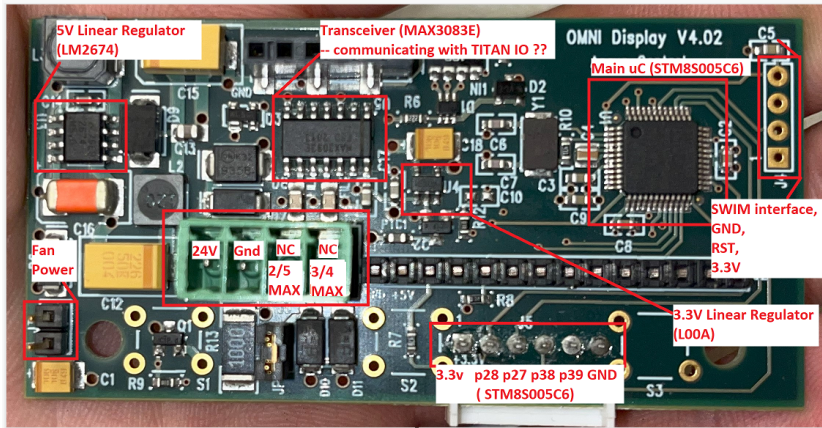


Figure 2.4: Argus Omnisensor microcontroller board with annotations describing key components which connects to the sensor board (Figure 2.5) to perform sensor readings and pass sensor data upstream.

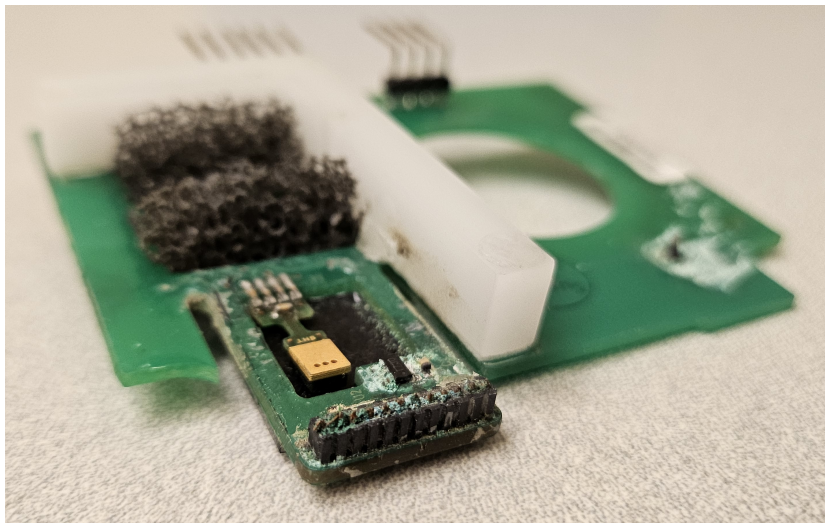


Figure 2.5: Argus Omnisensor sensor board which interfaces with the microcontroller board (Figure 2.4) to provide temperature and relative humidity sensing capabilities.

readings closer to where they matter most, such as at individual plant canopy heights to determine the temperature and relative humidity that each plant experiences. In addition, the freedom from having to be tethered to a wired connection means that access to the plants for watering, moving, or general greenhouse navigation is not a hazard.

There are many long range wireless communication protocols that are also low-power. To list a few, LoRa [36], ZigBee [26] [19], and SigFox [23] are popular options in agricultural and environmental sensing. A common point between these long range wireless options is their tradeoff of increased range at the cost of data throughput. These long range protocols often have data rates measured in kilobits (or even bits) per second, but can transmit at distance exceeding a few miles.

For LoRa, the key technology that enables its long range is the use of spread spectrum communication. By using multiple frequencies, LoRa receivers can receive and demodulate signals even when it is below the noise floor (commonly cited at around -120 dBm [21]). For example, the Texas Instruments CC1125 LoRa chip boasts reception as low as -129 dBm [6].

2.6 Visible Light Communication

Visible Light Communication (VLC) is the use of visible light (typically between UV and IR) for communication. It is a form of optical wireless communication, and uses free space propagation of light (i.e. no fiber strand medium as seen in fiber optic network cables). VLC is especially compelling to agricultural and greenhouse

applications due to its ultra-low power, non-existent RF interference, stronger ability to transmit power to charge VLC-enabled devices, and high-compatibility with LED lighting. In wireless systems, the key limiting factor is often the power consumption of the wireless device, as traditional RF-based methods can draw hundreds of milliwatts during communication and thereby reduce operational lifespan significantly. With VLC (and complementary RF backscatter), the power draw is orders of magnitude less and solar energy harvesting is readily available.

In recent years, VLC has been widely considered to be a promising technology for secure, high-speed, and energy-efficient wireless data transmission. Current VLC systems typically employ On-Off Keying (OOK) to modulate transmissions due to OOK's simplicity. A description of how OOK works is presented in Section 2.6.1. However, OOK modulation is prone to noise and interference [30], limiting its robustness, especially in noise-challenged environments. In response, recent research has explored various strategies to enhance the resilience and efficiency of VLC systems, several of which are discussed below.

The PassiveLiFi system [24], developed by IMDEA Networks, stands out as a key contribution to VLC research. This system uses photovoltaic (PV) cells for downlink communication via OOK modulation, combined with RF backscatter for the uplink, showcasing an energy-efficient, hybrid approach to VLC. Interestingly, PassiveLiFi also employs Chirp Spread Spectrum (CSS) based up-chirps to provide an oscillator signal to mix into their RF backscatter uplink. (See Section 2.6.2 for more details on the principles behind CSS.) An up-chirp is a signal whose frequency increases over time, and a down-chirp is a signal that has a decreasing frequency over time. In many cases, including

PassiveLiFi’s implementation [24] and also in the system discussed in this thesis, linear chirps are used. However, in PassiveLiFi’s system the data payload transmission still relies on OOK, which remains vulnerable to ambient noise.

Also developed by IMDEA Networks, the OpenVLC 1.4 open-source VLC platform [16], despite achieving high data rates under controlled conditions, continues to rely on OOK modulation, making it less resilient in noisy environments. Similarly to my current hardware implementation (see Section 3.4.2), OpenVLC also utilizes the BeagleBone Black (BBB) single-board computer for VLC transmission, although it employs a photodiode-based receiver paired with a singular high-power LED transmitter.

PassiveVLC builds upon the RetroVLC architecture [20], which achieves 1 kbps data rates through innovative use of low-power VLC techniques. In particular, RetroVLC enables duplex VLC transmission by toggling a liquid crystal shutter at the receiver to reflect light back to the transmitter. While these systems emphasize low-power operation, their modulation techniques do not directly address the issue of noise resilience.

Other approaches, such as POLI [8], utilize Polarized Light Intensity modulation with RGB lenses to transmit data to a camera. LuxLink [3] also focuses on low-power VLC but puts emphasis on the transmitter. While these methods introduce novel modulation techniques and optical components, they do not primarily aim to enhance the robustness of VLC against ambient noise.

Advanced optical techniques are further explored in ChromaLux [13] and SpectraLux [4], where ChromaLux employs liquid crystals and birefringence for VLC, and SpectraLux uses a spectrometer receiver alongside an ambient light liquid crystal shutter

transmitter. Although these studies advance VLC technology, they do not focus on the critical challenge of noise resilience that my work addresses through CSS modulation.

Additionally, in [31], a “zero energy” VLC receiver is proposed that focuses on embedded applications. It explores the dual use of photovoltaic (PV) cells for data reception and energy harvesting, relying on OOK modulation. While this approach is innovative in terms of energy efficiency, it remains limited by the noise sensitivity inherent to OOK, highlighting the need for more robust modulation techniques.

Although there have been significant advances in VLC technology, particularly in low-power operation, novel modulation techniques, and energy harvesting, the challenge of enhancing signal robustness, especially in noisy environments, remains. Addressing this challenge is the focus of my work in this thesis.

2.6.1 On Off Keying

On Off Keying (OOK) is a form of amplitude shift keying in which there are only two amplitude levels: high and low. The simplicity of OOK makes it attractive as a basic short range communication method. However, as it is an amplitude-based modulation technique, OOK is significantly influenced by noise, resulting in high bit error rates (BER). BER is a metric used to evaluate the ability of a link to transmit data without error, and is expressed as a percentage of incorrect bits over total bits sent. OOK is often adopted in VLC systems due to its simplicity (such as in [24]) and because the systems are often targeted towards indoor applications where the ambient noise is low. Another reason for its draw is because in indoor scenarios where the ambient light is low compared to outdoor conditions, high noise immunity is not a hard requirement.

2.6.2 Chirp Spread Spectrum and LoRa

Chirp Spread Spectrum (CSS) is the use of changing-frequency “chirps” to transmit symbols. A common protocol which uses CSS is LoRa due to its robustness to noise, but it is also possible to implement CSS in visible light communication. The implementation of CSS in VLC is a core contribution of this thesis.

A key concept within CSS spectrum is the idea of spread factor. Spread factor is a variable which determines the number of unique symbols that the bandwidth is divided into. For example, with a spread factor of $SF = 8$, there are $2^{SF} = 256$ symbols. For LoRa, the spread factor is commonly set between 7 and 12. In LoRa, spread factor also determines the symbol period and data rate of the channel.

One interesting impact of increasing the spread factor is that the BER decreases (if the symbol period remains constant). This is because as the spread factor increases, the number of bits per symbol also increases. Consider a single bit error in the case of $SF = 12$ versus the case of $SF = 7$. When a single bit error occurs, the BER is now $\frac{1}{12}$ instead of $\frac{1}{7}$.

Deploying a CSS-based optical communication system, originally designed for RF communication, poses significant challenges due to the need to ensure the demodulator is able to reliably interpret incoming signals. I address the challenges of designing and implementing a wireless link based on visible light to meet the high noise resilience required in greenhouses in Chapter 3. I describe my CSS implementation for FIAT LUX in Section 3.1. FIAT LUX’s performance evaluation is presented in Section 3.5.

Chapter 3

Design, Implementation, and Evaluation of FIAT LUX's Downlink

3.1 Specific Background on VLC and CSS

As mentioned in prior sections, CSS has not yet been applied towards VLC to carry data. This is mostly because most VLC applications are targeted to indoor environments where the ambient noise is generally ten times less than that of outdoor sunlight (e.g. 500 lx indoors versus 5000 lx outdoors). The large amount of wide spectrum noise from sunlight makes amplitude based modulation schemes ineffective due to their SNR requirements. For example, in PassiveLiFi [24] the conditions of their tests were only under 500 lx (indoor conditions) where they achieved ranges under 4 meters. In an outdoor environment, the expected ambient light would be around 5000 lx, which would completely drown out the signal.

Therefore, a target environment that is outdoors is not well-suited for am-

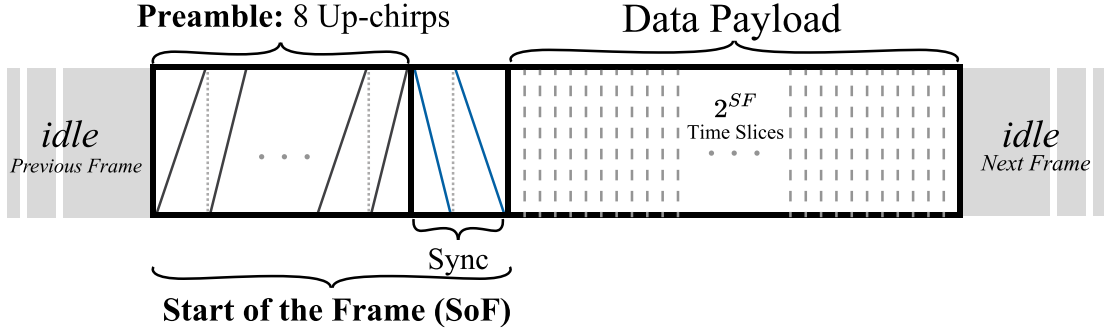


Figure 3.1: The proposed CSS frame adapted for optical communication.

plitude based modulation. Knowing this, my work has focused on applying spread spectrum techniques to VLC in the form of adapting CSS as seen in LoRa to VLC. I anticipated that implementing CSS in VLC would allow for communication under long range or high noise conditions. This is particularly well-suited for VLC in greenhouses which experience large amounts of sunlight.

As illustrated in Figure 3.1, a standard CSS frame consists of a Start of Frame (SoF) field, which includes a preamble with eight up-chirps, followed by a synchronization section with two down-chirps and the data payload. In FIAT LUX, we adopted this simple frame structure to avoid unnecessary overhead.

To determine whether the received signal follows a chirp pattern, I employ the *Is_Chirp* boolean condition, which checks for the characteristic frequency sweep indicative of chirp modulation. This condition effectively distinguishes chirp signals from noise or other non-chirp modulations within the received data. The pseudocode in Algorithm 1 describes the demodulation process.

The demodulator initiates its procedure by entering an idle state, where it

Algorithm 1 Chirp Spread Spectrum demodulator pseudocode

for Each frame-wide window of samples $S = \{P(f_i, t_i)\}_i^n$ containing frequency and

time tuples (f_i, t_i) **do**

 Apply *Is_Chirp* to S

for 8 consecutive preamble symbols **do**

if Modulus of consecutive points $P(f_i, t_i) < \beta$ **then**

 Failed to detect preamble, advance S and restart from step 1

end if

end for

for 2 consecutive sync down-chirp symbols **do**

 Wait for the down-chirps to expire

end for

for Each payload symbol **do**

 Mark points of interest (PoI) based on significant frequency transitions within
each symbol

 Demodulate the symbol into bits using the locations of the PoI

end for

end for

applies the *Is_Chirp* condition to $S = \{P(f_i, t_i)\}_i^n$, a sample of n data points. The purpose of the *Is_Chirp* condition is to determine if the sample belongs to a chirp by analyzing the linear behavior of the collected datasets, which should correspond to the expected line slope. To achieve this, I define two integrals: Expected $I_{Expected}$ (Eq. 3.2) and Actual I_{Actual} (Eq. 3.3). By comparing the modulus of the difference between these integrals with a threshold value α (Eq. 3.4), the *Is_Chirp* condition verifies whether the given data points form part of a chirp. Upon detecting a chirp, the demodulator transitions to parsing the preamble.

To calculate $I_{Expected}$, I need the expected slope of a chirp, which will be calculated based on the Max and Min frequency and the time period ρ for each chirp. (Eq. 3.1)

$$\exists p_i \in P \tag{3.1}$$

$$I_{Expected} = \int_{S_{Start}}^{S_{end}} \left(\frac{max_freq - min_freq}{\rho} X + min_freq \right) dX \tag{3.2}$$

$$I_{Actual} = \sum_{i=S_{Start}}^{S_{end}-1} \int_i^{i+1} \left(\frac{P_i(f) - P_{i-1}(f)}{P_i(t) - P_{i-1}(t)} \cdot X + P_{i-1}(t) \right) dX \tag{3.3}$$

$$Is_Chirp : |I_{Actual} - I_{Expected}| \leq \alpha \tag{3.4}$$

In Figure 3.2, I illustrate a chirp detection method in a noisy environment using an actual up-chirp, where the purple line represents the noisy signal and the solid black line represents the expected chirp. By collecting a sample S and applying the *Is_Chirp* condition, I can determine whether the captured data points are noise or part of the up-chirp.

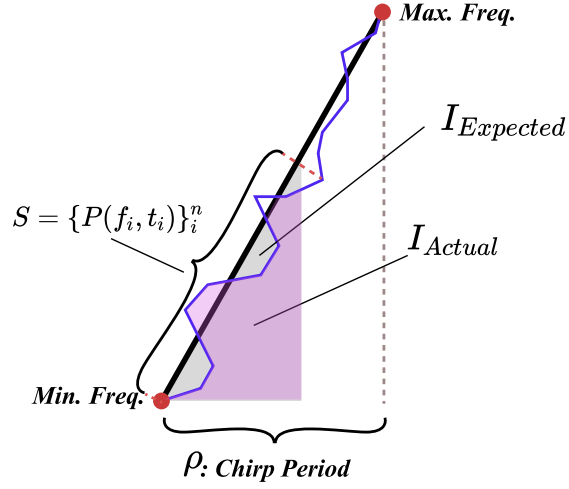


Figure 3.2: Illustration of chirp detection in a noisy environment.

The demodulator captures the received data points as tuples of frequency f and time t , which I denote as $P(f, t)$ and refer to as points. Upon entering the preamble section of the frame, the demodulator detects the number of chirps by comparing the absolute value of the difference between the current point's frequency $P_t.f$ and the next point's frequency $P_{t+1}.f$, against a predefined threshold β , which is determined based on ambient noise levels. If the modulus is greater than or equal to β , indicating a decrease in frequency, it is interpreted as the detection of a single preamble. This process is repeated seven times, as 8th and final up-chirp signifies the beginning of the first down-chirp in the synchronization phase.

$$\{\exists p \in P \mid |p_{t+1}.f - p_t.f| < \beta\} \quad (3.5)$$

It is important to note that the value of β is configured according to the environment's ambient noise level. To determine β , I transmit multiple frames to the

receiver device and adjust β until there is minimal error in chirp detection.

In the demodulator's payload state, I consider Points of Interest (PoIs) within a CSS symbol that are identified based on significant frequency transitions observed during symbol changes, particularly sharp frequency increases and decreases. To differentiate these frequency transitions from noise, the minimum detectable frequency rise or drop is computed by Eq. 3.6.

$$Minimum_transition = \frac{Max_freq. - Min_freq.}{2^{SF}} \quad (3.6)$$

Frequency transitions smaller than the *Minimum_transition* threshold are considered noise and are discarded. When a rise or drop exceeding this threshold is detected, it is marked as a Point of Interest (PoI). These PoIs are then classified according to the CSS symbol structure into one of three categories: initial offset, chirp overflow point, or final symbol offset.

After identifying and labeling the PoIs, the expected symbol can be computed based on the PoI type: initial offset, overflow, or final offset. The corresponding formulas for each type are provided below. For each chirp period within the symbol, three PoIs are utilized to determine the symbol value. Each PoI corresponds to one of the three critical points in the chirp period, enabling precise determination of the symbol value based on the observed PoIs.

$$Initial_Offset : \frac{PoI_freq. * 2^{SF}}{Max_freq. - Min_freq.} \quad (3.7)$$

$$Chirp_Overflow : \frac{PoI_time * 2^{SF}}{Chirp_Period} \quad (3.8)$$

$$Final_offset : 2^{SF} - \frac{PoI_freq. * 2^{SF}}{Max_freq. - Min_freq.} \quad (3.9)$$

3.2 VLC System Overview

A block diagram describing the VLC system is shown in Figure 3.3. There are three main components of the system, whose network hierarchy is a tree. The “Modbus Wireless Passthrough” acts as the head node, and is the sole interface between each greenhouse’s “Sensor Manager” and the Argus Controls software (through the ISODN). The “Modbus Wireless Passthrough” exists to gather data from downstream sensor managers and expose modbus registers to the upstream Argus. Each greenhouse must have a “Sensor Manager” which manages the VLC downlink through the greenhouse LEDs and provides a RF backscatter uplink through a universal software radio peripheral (USRP). The “Sensor Manager” acts as the local access point for each greenhouse’s many “IoT Tag” sensor boards. Finally, each greenhouse may have multiple “IoT Tag” sensor boards to obtain readings at specific user-specified locations within a greenhouse, such as near the canopy height of the plants, or at the soil of each planter.

In this chapter, I will focus on the VLC downlink portion of the system, which is described in Figure 3.3. This portion of the overall system consisted only of the key VLC downlink components, and is titled FIAT LUX. This included the Sensor Manager, the LEDs, and the IoT Tag (minus the RF backscatter), as shown in Figure 3.4.

3.3 Interfacing with the XtremeLUX LEDs

One of the major benefits of using VLC in greenhouses is the reuse of existing LED grow lights instead of having to wire up a new set of LEDs specifically for VLC. In the UCSC Coastal Science Campus, the LED grow lights in use are the XtremeLUX

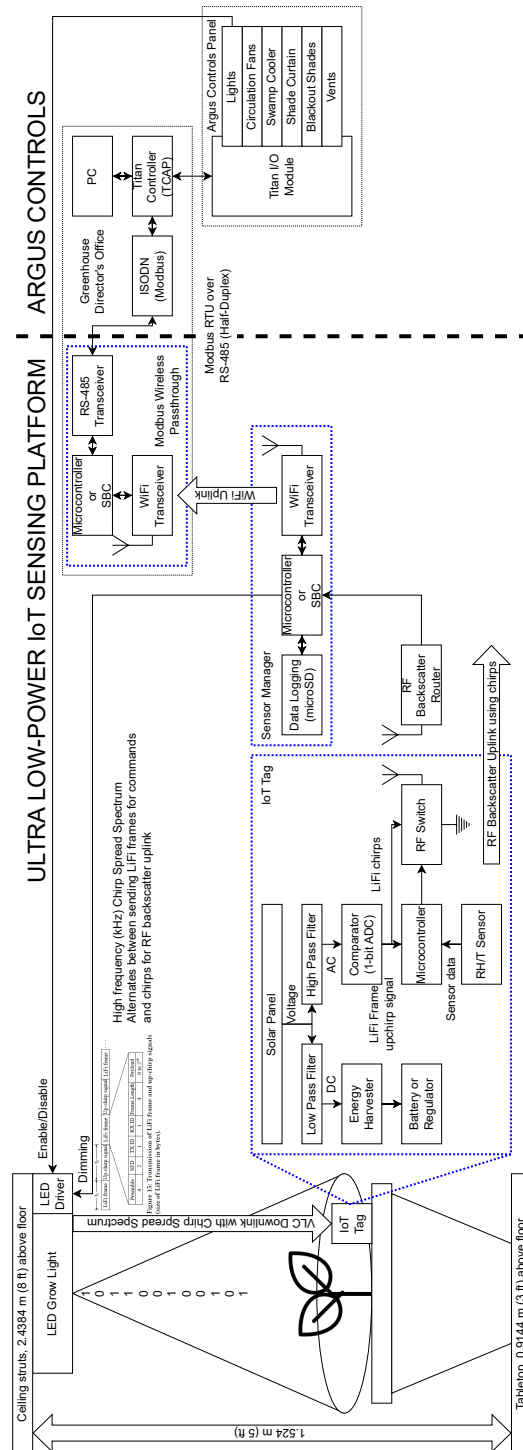


Figure 3.3: Novel VLC system diagram. Of this system, the communication downlink between the Sensor Manager and the IoT Tag was built and evaluated in FIAT LUX.

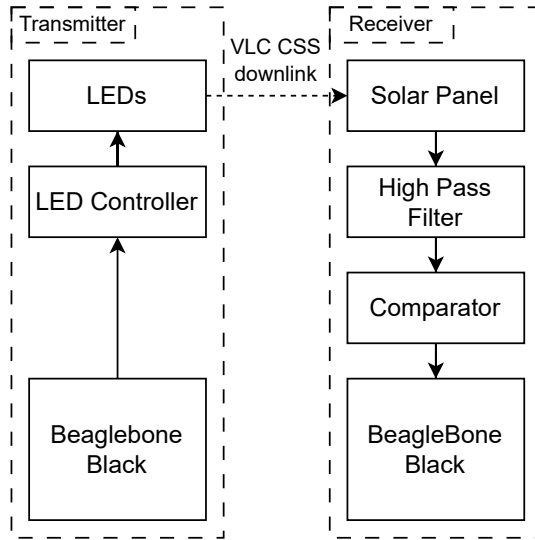


Figure 3.4: FIAT LUX’s architecture and functional components.

LF11 (Light Fixture 11) and the LBRB9 (Light Bar Red Blue 9). The LF11 is a combination of five individual light bars with varying output wavelengths within the PAR regime [41]. These light bars are daisy-chained using I2C for communication, and have a maximum combined draw of 564 watts. The LBRB9 is a single light bar which is attached to the LF11 and has a maximum draw of 52 watts. Instead of having an I2C connection, this light bar has two analog inputs (0V - 5V) to vary the brightness of its red and blue channels. The LF11 is used for providing the bulk of the plant illumination, while the LBRB9 provides additional illumination and also VLC to the sensor tags.

To control the LF11 light fixtures, BBB must connect to a DC11 LED controller. However, the DC11 controller only has a RS-485 interface, which is a serial interface using differential signals suitable for long-distance industrial controls. In order to bridge between the BBB and the DC11 controller, I used a BF-430 TCP/IP to RS-

485 converter. This allowed us to use the `telnet` remote access program on the BBB to control the LEDs' intensity, scheduling, and more. For control of the single LBRB9 LED bar that modulated the VLC downlink, I tapped into two analog 0V - 5V lines. By outputting a 5V PWM signal (level-shifted up from the BBB's 3.3V output), I was able to control the LED's full dynamic output range with high speeds.

On the BBB, I originally developed the VLC code in userspace where the execution thread competes with other threads for CPU time. This led to uncertain timing which caused the output chirp signals to not be linear as the PWM control code would not have guaranteed timing. To alleviate this, I shifted to use one of the BBB's two coprocessors, also known as the Programmable Realtime Units (PRU). The PRUs are essentially independent baremetal microcontrollers that have communication channels with the main CPU and access to nearly all peripherals. The PRUs do not service Linux threads for the main CPU, and are therefore a good option for timing-sensitive tasks or peripheral interfacing tasks. To this end, I moved the low-level chirp code to the PRU to allow us to have dedicated guaranteed-timing chirp transmission and chirp reception. Higher layer tasks such as chunking data into packets or reforming files from multiple packets is relegated to a userspace program which hooks up to the communication channel between the PRU and main CPU called the PRU mailbox.

3.4 Experimental Methodology

I tested, validated and evaluated FIAT LUX using both MATLAB simulations and real-world experiments. The goal was to demonstrate that using a CSS-based down-

link yields higher noise immunity than OOK-based approaches. Consequently, longer communication range as well as improved robustness and reliability can be achieved.

In the experimental study, I used BER as the main performance metric. To demonstrate FIAT LUX’s noise immunity and longer communication range, I measured BER under a variety of lighting conditions and at multiple distances.

In FIAT LUX’s current prototype implementation, I used solar panels to capture LED-generated signals (see Figure 3.4). To record the amount of ambient lighting and the light signal strength at various distances, I used a handheld lux meter [32]. In the ambient noise experiments, I used an XtremeLUX LF11 light fixture which consists of a combination of LEDs outputting a mixture of visible wavelengths to adjust the amount of background illumination.

3.4.1 Simulation

In the simulations, I considered two sources which could affect the SNR, that being sunlight and path loss. I added additive white Gaussian noise (AWGN) to model noise from sunlight. For path loss modeling, I used the free space path loss relationship [18], which is proportional to $1/d^2$ with a scaling coefficient in order to correct for other noise sources in the environment and match the conditions in the test environment.

CSS in wireless communication is achieved by adjusting the phase of a chirp signal to provide unique symbols. When adapted to VLC, it could likewise be achieved by varying the frequency of light flashes over time. I simulated CSS and OOK modulation and demodulation, and compared their performance by calculating the BER across various symbol frequencies, noise levels, spreading factors, and distances.

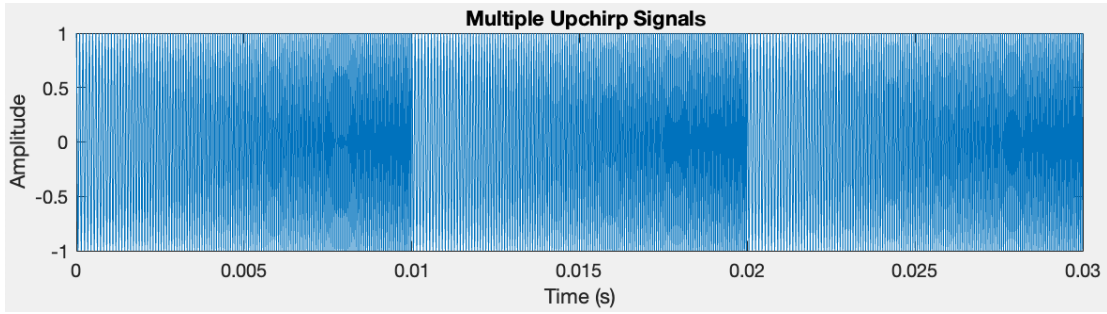


Figure 3.5: Time domain representation of three example chirp signals.

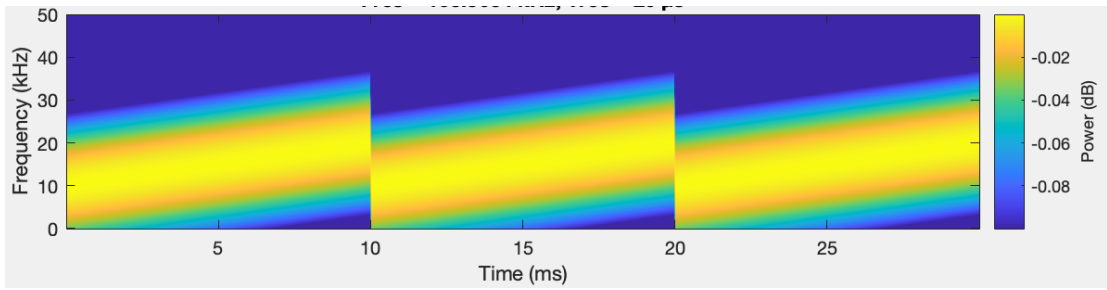


Figure 3.6: Spectrogram representation of the three example chirp signals shown in Figure 3.5.

The formula for an up-chirp starting from frequency f_0 is $s(t) = e^{j*2\pi(\beta/2*t^2+f_0*t)}$, where β is the frequency variation slope given by the ratio between bandwidth (BW) and time symbol T_{symp} . ($\beta = BW/T_{symp}$). Figure 3.5 shows three up chirps in the time domain created by the MATLAB simulation. To verify it is able to be demodulated by doing FFT as LoRa [10] techniques do, a corresponding spectrum is shown in Figure 3.6.

I used MATLAB to model OOK and CSS as described in Figures 3.7 and 3.8 respectively. The general signal path is to generate the transmitted signal based

OOK modulation and demodulation

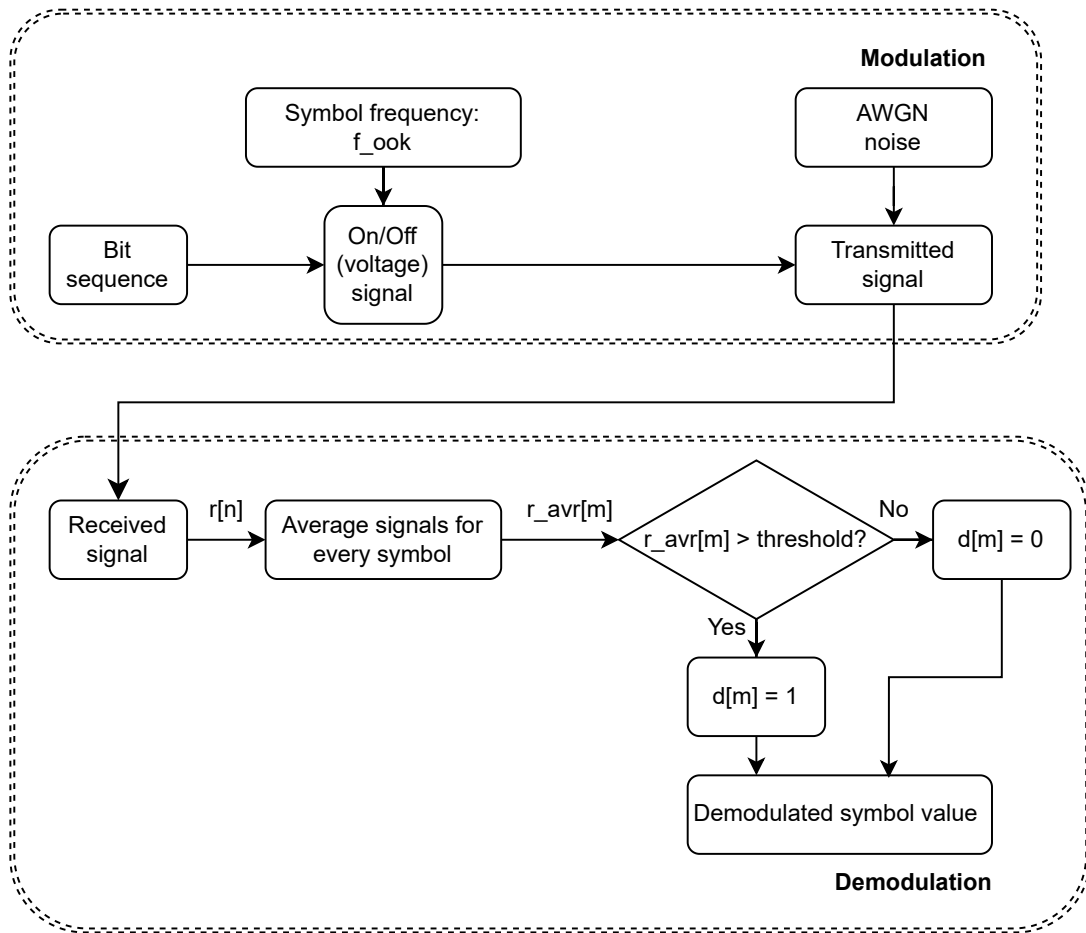


Figure 3.7: Simulation workflow for modulation and demodulation of an OOK VLC signal. $r[n]$ represents the array of received samples, $r_{\text{avr}}[m]$ is the sliding window average, and $d[m]$ is the corresponding '0' or '1' obtained from the average being above or below the set threshold.

CSS modulation and demodulation

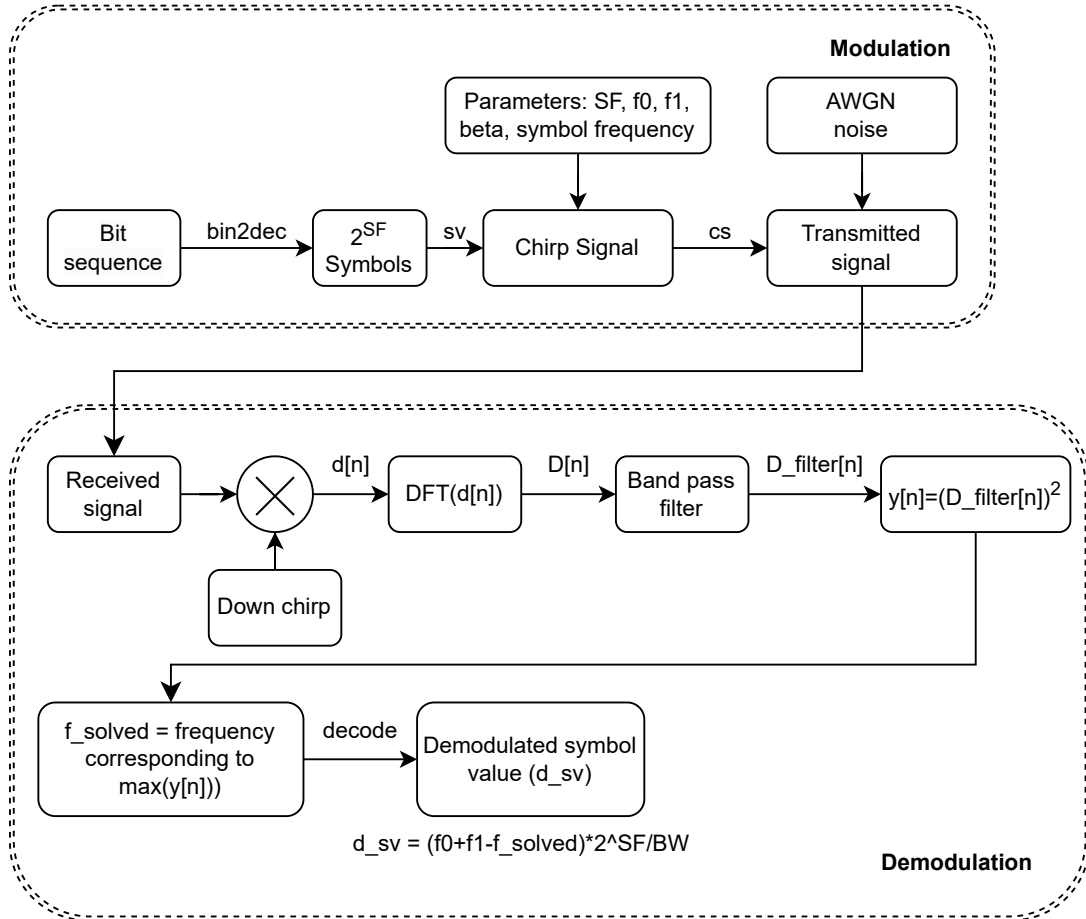


Figure 3.8: Simulation workflow for modulation and demodulation of a CSS VLC signal. sv represents the symbol value being evaluated, cs is the corresponding chirp for the selected symbol value, $d[n]$ is the received samples multiplied with the base down-chirp, $D[n]$ is the frequency content of the time-domain signal, and $D_filter[n]$ is the frequency content of that signal after applying a bandpass filter to remove unwanted low and high frequency noise.

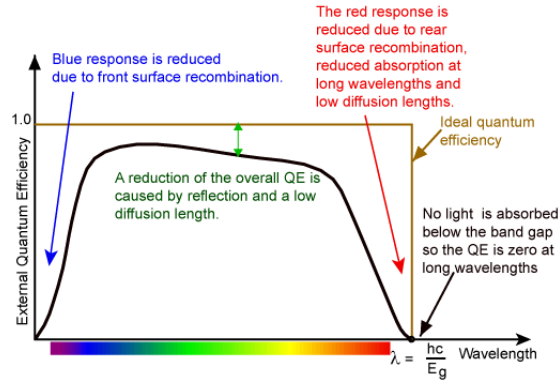


Figure 3.9: Typical quantum efficiency of a PV cell. The PV cell’s response to red and blue wavelengths is reduced, and is most active in the center of the 400 nm to 700 nm range. Image retrieved from [28].

on the input binary pattern, factor in path loss to the received signal, and perform demodulation on the received samples.

3.4.2 FIAT LUX Prototype

Because FIAT LUX was originally motivated by greenhouse applications, the transmitter being used in FIAT LUX’s current prototype is an XtremeLUX Sun Deputy LBRB9 light fixture. This LED array has two independently controllable channels, one emitting deep red (663 nm) and the other emitting deep blue (455 nm), both of which are maximally absorbed by chlorophyll. However, the narrow spectra in which the LBRB9 operates in is non-ideal for communication to a PV (photovoltaic) cell which is generally efficient throughout the center of the visible spectrum as depicted in Figure 3.9.

FIAT LUX’s receiver (Figure 3.10) utilizes an array of solar cells that feed into a high-pass filter and one-bit ADC, described in Figure 3.11. The solar cell array consists of four SM141K04LV solar cells in series in order to maximize peak-to-peak

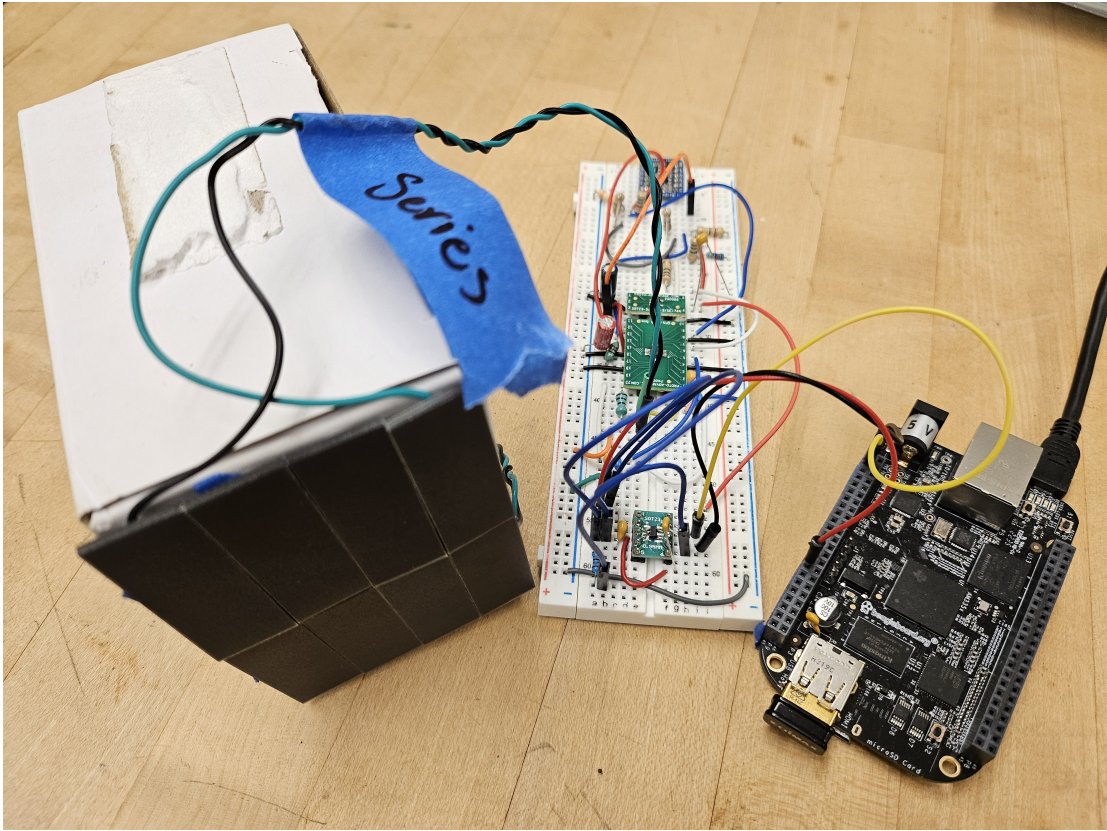


Figure 3.10: FIAT LUX receiver, which consists of a BBB, an analog optical front-end, and the solar panels. Experimental setup to evaluate the performance of the FIAT LUX receiver at distance. The transmitter light bar LBRB9 is oriented such that it is perpendicular to the receiver. The receiver is located on the left and is situated mid-height to the light bar.

output voltage. The SM141K04LV cell was chosen as a successor to the Pareto optimal SLMD121H04L presented in [24] for its increased power production capabilities. The passive high-pass filter is designed to reduce noise from ambient artificial lighting at 60 Hz. The comparator used for the FIAT LUX receiver is the TS881 whose propagation delay and internal hysteresis work well to eradicate the 100 KHz noise generated by the switching frequency of the LBRB9 LED bar.

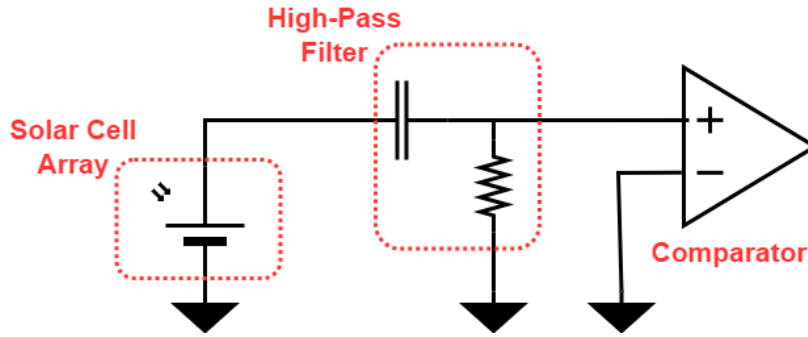


Figure 3.11: Fiat Lux receiver schematic.

The algorithms and equations presented in Section 2.6.2 were implemented and evaluated using datasets collected from a real-world laboratory setup. The transmission setup consisted of sending randomized ASCII strings at SF of 8, minimum frequency of 300 Hz, and maximum frequency of 3 kHz with a chirp period of 1 second. Test messages were transmitted using the LBRB9 light bar’s red channel at distance intervals of 0.25 meters, ranging from 0 to 4 meters. In addition, noise tests were conducted by using extra LED light bars from a XtremeLUX LF11 light fixture to adjust the amount of ambient noise.

I implemented the transmitter modulator and receiver demodulator using two BBBs. The Programmable Realtime Unit (PRU) onboard allows for deterministic low-level execution while the userspace Linux aids in high performance computing. For the modulator, a PRU program receives strings from userspace through a character device (`‘/dev/rpmsg_pru30’`). Inside the PRU, I use the pulse width modulation (PWM) subsystem to emit linear chirp signals, which are boosted up to 5V logic levels using an external 3.3V to 5V logic level converter. This is done for maximizing the LBRB9 output intensity swing. At the receiver end, the solar panel is connected to the TS881

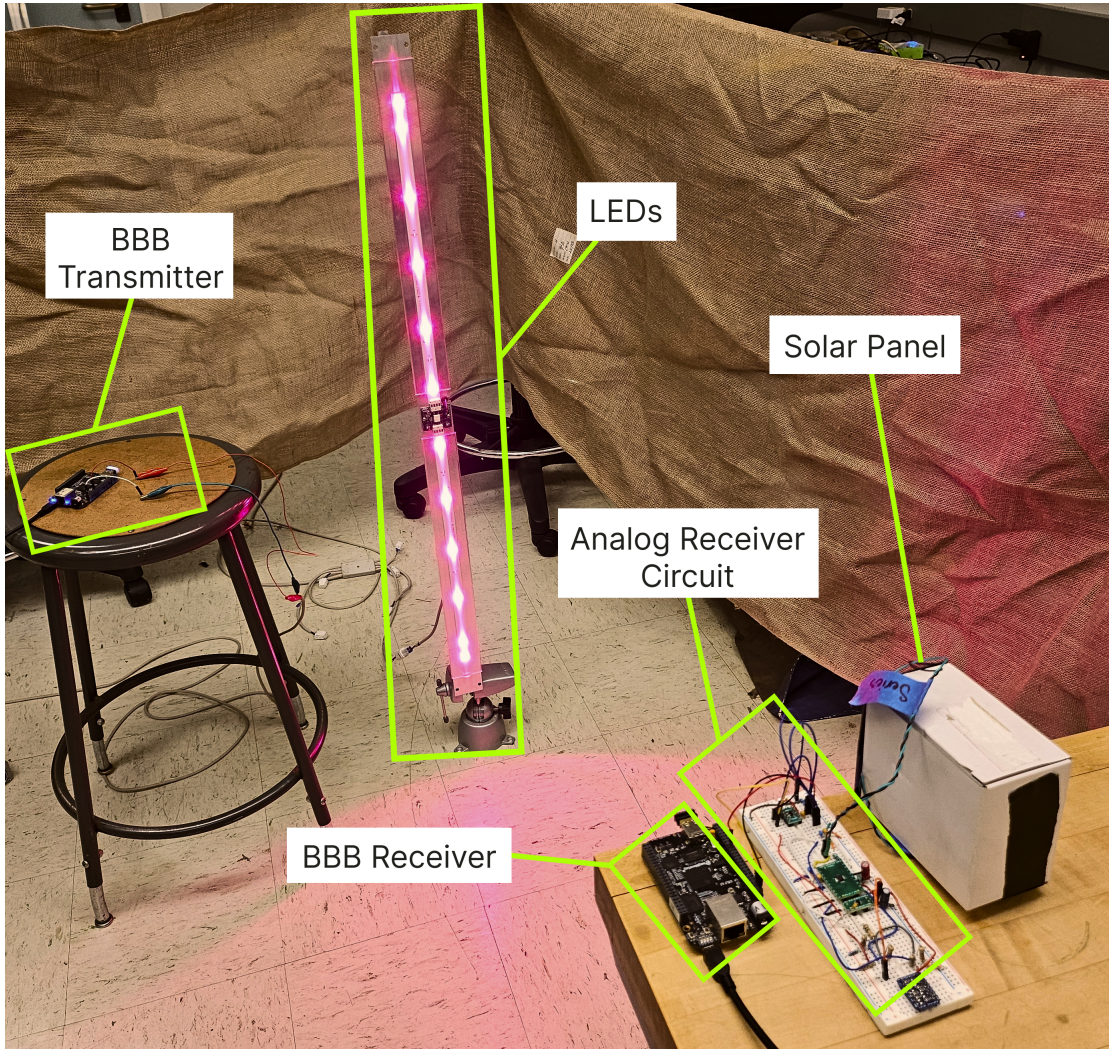


Figure 3.12: Experimental setup for evaluating FIAT LUX's range and noise resilience which is aligned with Figure 3.4

comparator. A GPIO pin connects the output pin of the TS881 comparator to the BBB. The PRU samples the pin and times the duration of each high pulse to calculate the instantaneous frequency. (Due to this method, these instantaneous frequency samples do not have even time spacings.) These frequency measurements are passed to a program in userspace which collects the samples and logs them to a CSV file. Later, the sample file is put through an offline demodulator which follows the demodulation methods described in Section 2.6.2.

The BER was calculated by comparing the number of erroneous bits to the total bit length of the transmitted message. Multiple tests were conducted for each distance with varying randomized messages, and the graphs discussed in Section 3.5 indicate the average error rates as a function of distance and ambient noise.

3.5 Experimental Results

Throughout the course of the project, I prototyped and evaluated the VLC link of the overall system, the results of which are under review for PerCom 2025. To evaluate FIAT LUX's performance, I provide comprehensive test cases that illustrate how CSS outperforms OOK. This is shown in Figures 3.13, 3.14, and 3.15. With these graphs, I pictured the resiliency of the VLC-adapted CSS in comparison to OOK. Further, I showed CSS can support higher distances before hitting the BER threshold.

3.5.1 FIAT LUX Prototype Results

The results of the demodulator algorithm, processed on the experimental datasets, are presented in Figure 3.13. This figure depicts the performance of FIAT

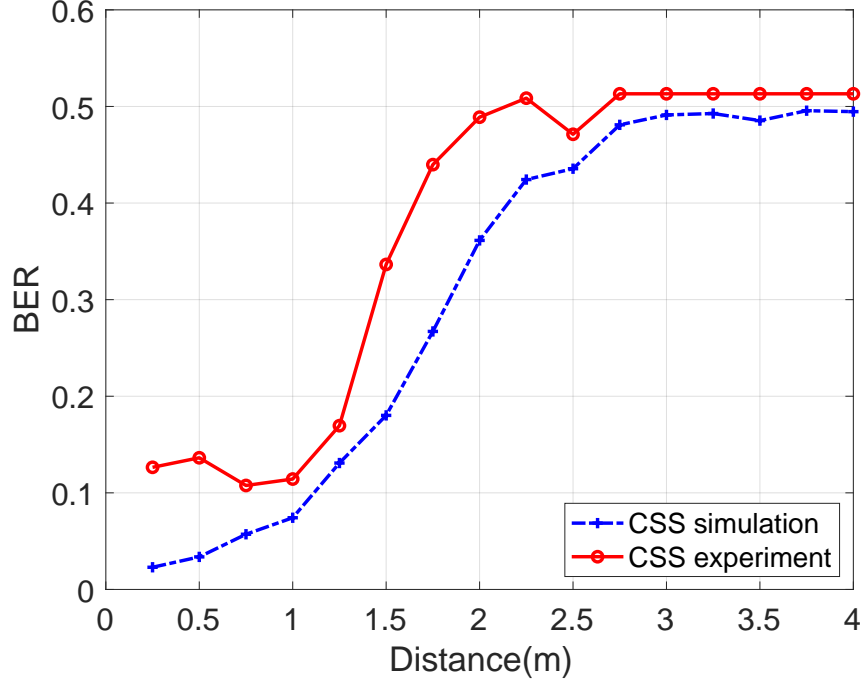


Figure 3.13: Comparison of simulated CSS versus experimental CSS implementation with $SF = 8$ between 0 and 4 meters. In the CSS experiment, no ambient noise was added (i.e. dark room).

LUX’s CSS demodulation over varying distances against the simulated results in dark room conditions. The graph illustrates the BER over distances up to 4 meters. The simulation curve follows the behavior of my real-world experiments closely, and I observe higher error rates in my experiment than in simulation. This can be attributed to the simulation only accounting for free space path loss, and not the influence of other factors that influence SNR, such as multipath effects, and scattering, and reflections.

One possible reason why the transmission range was low could be due to the mismatch between the spectral sensitivity of the solar panel and the wavelength of the LED as mentioned in Section 3.4.2. In addition, at close ranges the LED’s light can reflect off of the receiver and its own frame before hitting the receiver again. This could

cause additional noise at close range, which may explain the uptick in BER below the 0.5 meter mark.

In a separate experiment, I emulated outdoor conditions by increasing the amount of background illumination using the LF11 light fixture (as mentioned in Section 3.4.2). However, I was unable to successfully demodulate the signal when the background illuminance increased beyond 112 lx at a distance of one meter. For reference, the SNR of regular office lighting is approximately 250 lx.

The inability to demodulate and obtain BER below 50% in the emulated outdoor experiment could be due to multiple factors. Foremost is that the noise source (LF11 light fixture) was placed right beside the transmitter signal source (LBRB9 light bar). In previous tests conducted under indoor office light conditions using the $\tilde{250}$ lx office ceiling lights, I achieved indoor ranges up to approximately 2 meters. The main difference between these two environments is the location and orientation of the noise source. A noise source suspended from the ceiling and perpendicular to a horizontal-facing receiver's solar panel will experience noise of lower intensity than one that is placed normal to the receiver. The other factor that could be affecting the emulated outdoor experiment's performance would be the lens of the noise source. The LF11 light fixture has a transparent clear covering over its LEDs, which does not diffuse its light, whereas the office ceiling lights have an opaque diffuser. The diffuser's effect on the light could cause the light to scatter more widely and thereby reduce the noise power delivered to the receiver.

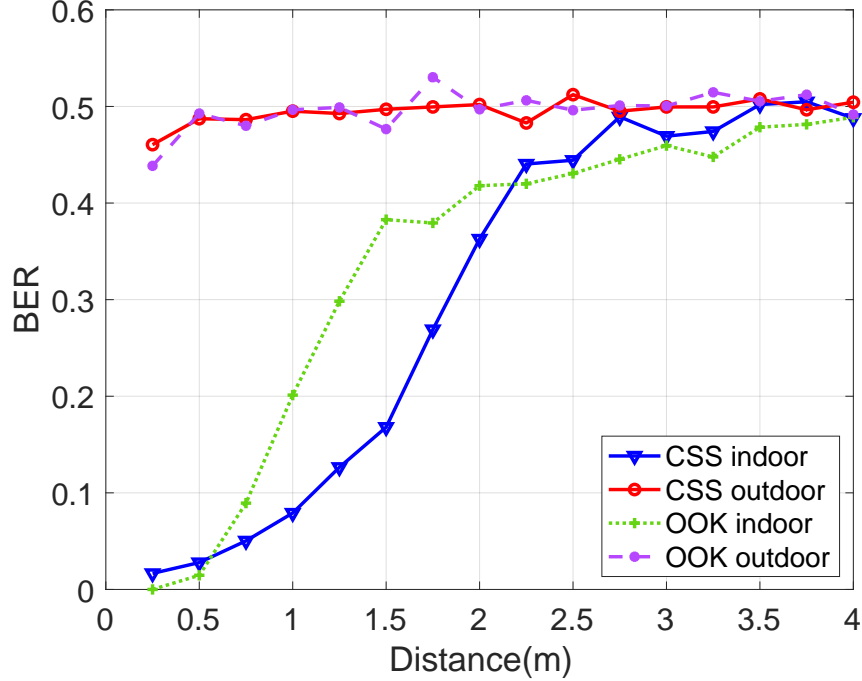


Figure 3.14: Simulation results which compare simulated OOK against simulated CSS at various distances and with $SF = 8$.

3.5.2 Simulation Results

In addition to simulating CSS at range, I also simulated OOK in indoor and outdoor noise environments. Figures 3.14 and 3.15 show the results of simulating CSS and OOK when distance and noise changes, respectively.

Figure 3.14 shows a closeup view of the first 4 meters of simulated CSS and simulated OOK. In this regime, I observe that the BER of CSS is lower than the BER of OOK in the indoor case. This shows that CSS is more suitable than OOK at range under indoor lighting conditions (approximately 250 lx).

I expected to observe a working link for CSS at short outdoor distances, but the performance of both CSS and OOK are near the 50% BER limit in the outdoor case

above 0.25 meters. In the outdoor regime, I applied AWGN equivalent to about 2500 lx of sunlight, which is approximately -30 dB given the strength of the signal. I observe BER saturation here due to overestimating the amount of background noise. The -30 dB outdoor SNR was derived from $SNR = 20 \log \frac{55\text{lx}}{2635\text{lx}} = -33.6\text{dB}$, where the signal and noise lux readings were gathered at a local greenhouse at mid-day. During other times of day and depending on weather, the amount of outdoor noise may vary. From the results of the outdoor simulations, the system did not meet my initial expectations for the system's performance. In Chapter 5, I discuss in more depth the directions in which I may adjust the model to better reflect my understanding of the system.

In the indoor regime where the background lighting is approximately 250 lx (and consequently $SNR = 20 \log \frac{365\text{lx}}{120\text{lx}} = +9.6\text{dB}$), the output of the simulated CSS here closely matches what I observed in reality as corroborated in Figure 3.13.

The last set of simulations in Figure 3.15 show the BER of OOK and CSS with different spreading factors ($SF = 7, 8, 12$) as the amount of background noise increases. I observe that higher SF results in a lower BER for CSS, and CSS at the selected spreading factors outperforms OOK. The simulation results are consistent with my expectations, showing that the CSS modulation method could improve the robustness to environmental noise. I also evaluated the BER versus the chirp bandwidth, but did not find any appreciable difference.

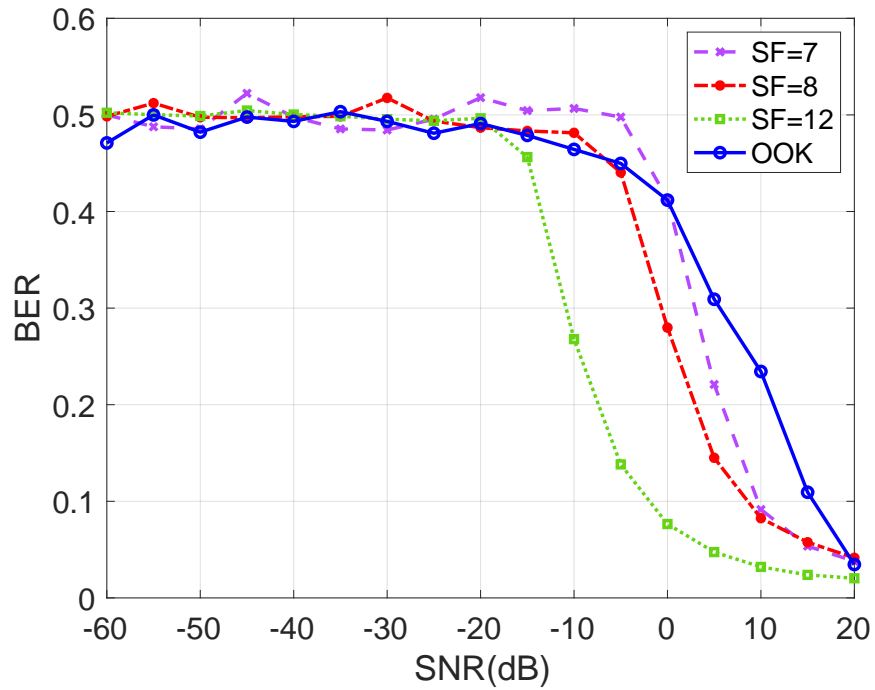


Figure 3.15: Simulation results which compare simulated OOK against simulated CSS (with $SF = 7, 8, 12$) under various amounts of ambient light. The amount of ambient light added to the signal is expressed here in terms of SNR at the receiver. For reference, in FIAT LUX SNR indoors is approximately +10 dB, while the SNR outdoors is approximately -30 dB (at 1 meter with the LBRB9 LED and SM141K04LV solar panels).

Chapter 4

Greenhouse Integration

4.1 Traditional IoT System Overview

In the early stages of the project, I wanted to be able to deploy a wireless sensor network (which resembles a traditional IoT system) that could interface with the pre-existing Argus system. This wireless sensor network would serve as a mid-way comparison point between the wired Argus system and the novel low power visible light communication system. In addition, the development of the traditional IoT system would provide helpful insights on how the novel VLC deployment can communicate with the Argus infrastructure.

4.2 Design and Implementation

A system diagram of the traditional IoT system is shown in Figure 4.1. The key components of the traditional IoT system are the “IoT Tag” sensors and the sole “Sensor Manager”. The purpose of the sensor manager is to collect the sensor information

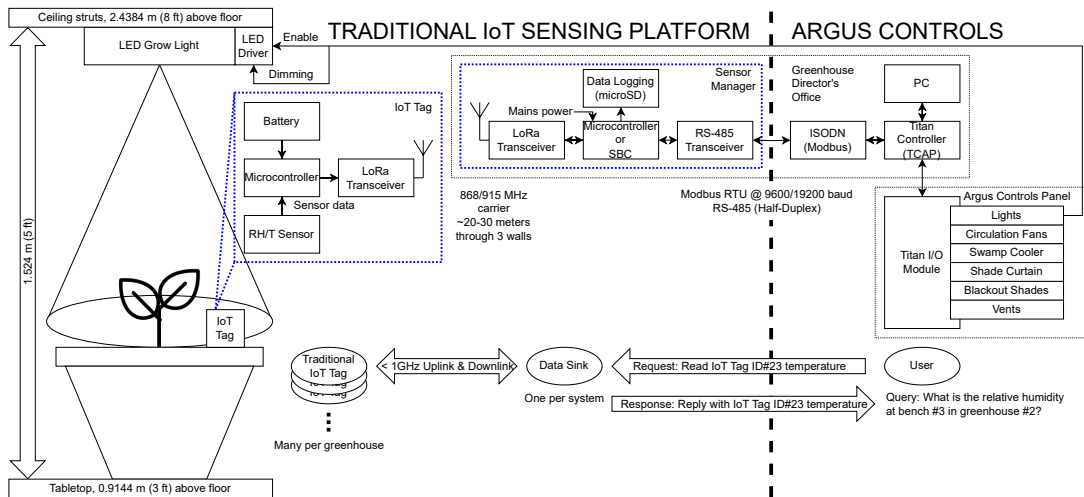


Figure 4.1: System diagram for the traditional IoT deployment. The two main components developed in this chapter are the IoT Tag and the Sensor Manager.

gathered from multiple sensor tags and prepare the formatting of the data for the Argus Controls side of the system to the right of the vertical dashed line. The IoT sensor tags use a microcontroller to gather the temperature and relative humidity, which are sent to the sensor manager wirelessly.

It is important to note that a portion of the work described in this section was conducted by my colleague Matt Kaltman. In order to better understand the work, I present the system in its entirety and will note where and to what extent Matt contributed to the success of the greenhouse integration. Matt performed work on the IoT sensor tag including all MSP430 microcontroller code, low power optimizations, and peripheral control, including a final all-in-one printed circuit board design. Essentially, this is everything to the left of the wireless link between the IoT Tag and the Sensor Manager in Figure 4.1. My contributions included all BBB code, device networking,

Modbus interfacing, and peripheral control. My work is described by everything to the right of the division between the IoT Tag and the Sensor Manager in Figure 4.1. We both met in the middle to settle on a packet structure and other details pertaining to the wireless LoRa link.

4.2.0.1 MSP430 Sensor Tag

The sensor tag uses a MSP430FR5969 microcontroller, which was chosen by Matt for its low power consumption and non-volatile memory. Low power consumption is a must for any power-constrained system such as wireless sensors to extend battery lifespan, while the non-volatile memory prevents data loss in the case of deep sleep power duty cycling to further reduce power consumption. The HDC2021 sensor provides temperature and relative humidity over I2C to the MSP430, and was initially chosen by Matt to be as similar to the capabilities as the Argus Omnisensor for the purpose of side-by-side performance characterization. A CC1125 LoRa transceiver allows bidirectional communication between the sensor tag and the sensor manager. I evaluated multiple wireless transmission options but ultimately chose to use LoRa due to its ease of use and low power.

4.2.0.2 BBB Sensor Manager

On the sensor manager side, a BBB is used to poll and collect the latest temperature and humidity readings from the sensor tags. I chose the BBB because I needed an embedded Linux environment to allow for wireless networking, remote access, file handling, and a simple interface with the Argus Controls ISODN. The same CC1125

LoRa transceiver used in the sensor tag provides the BBB with point-to-point wireless communication with each sensor. After receiving sensor data, the BBB saves a backup file containing the sensor readings to a local microSD card for offline data analysis. At the same time, a USB to RS-485 cable allows the BBB to expose its Modbus registers which contain the newly updated sensor readings to the Argus system. Finally, a USB WiFi adapter is used to provide remote management and configuration capabilities.

4.2.1 Argus Interface

One of the challenges with designing the custom communication and sensing platform is integration with pre-existing infrastructure. In the case of the UCSC greenhouses, this required interfacing with the Argus Controls ecosystem.

Fortunately, Argus provides a method to connect external third party devices. This is done through a special Argus hardware module called the Isolated Device Network Board (ISODN). The ISODN is intended for connecting legacy Argus sensors to modern Argus infrastructure, but can also be used to support RS-485 based networks such as Modbus RTU or eBUS [9].

To interface the BBB coordinator to the Argus, I used a USB to RS-485 cable from FTDI (USB-RS485-WE-1800-BT). This cable allows for bidirectional communication between the BBB and the Argus by converting the PHY between USB and RS-485. One of the primary reasons why I chose to use the USB to RS-485 cable was because of its ease of use on the BBB side, as it appeared as a simple character device (e.g. `/dev/ttyUSB0`) which can be written to and read from without having to manage custom buffers as it relied on the buffers provided through the BBB's USB device interface.



Figure 4.2: Argus Isolated Device Network Board (ISODN). The ribbon cable connects the ISODN with the Argus control panel. The screw terminal connects the ISODN with the BBB via a USB to RS-485 cable. Image retrieved from [9].

With the RS-485 cable connected to the Argus ISODN, the PHY connection was established. To connect a Modbus device such as the BBB coordinator, it must not only connect over RS-485 to the TCAP’s ISODN, but it also must have its address, registers, and polling settings pre-configured within the Argus control software. I chose to use Modbus via the open source libmodbus library ¹ to provide the sensor data in a Modbus-compliant format for the Argus control software to read. Modbus is somewhat similar to I2C in that the server device (such as the BBB coordinator) exposes a set of registers to the client (such as the Argus control panel shown in Figure 4.3) through a process called mapping, and the client may choose to read from or write to the server’s registers according to the function code it sends in the Modbus packet. I exposed four registers per downstream relative humidity and temperature sensor, two of which hold the relative humidity and temperature in their raw sensor reading format, while the other two registers hold the converted values as floats representing percent relative humidity and degrees Celsius. Some mathematical and bitmasking operations

¹<https://github.com/stephane/libmodbus>

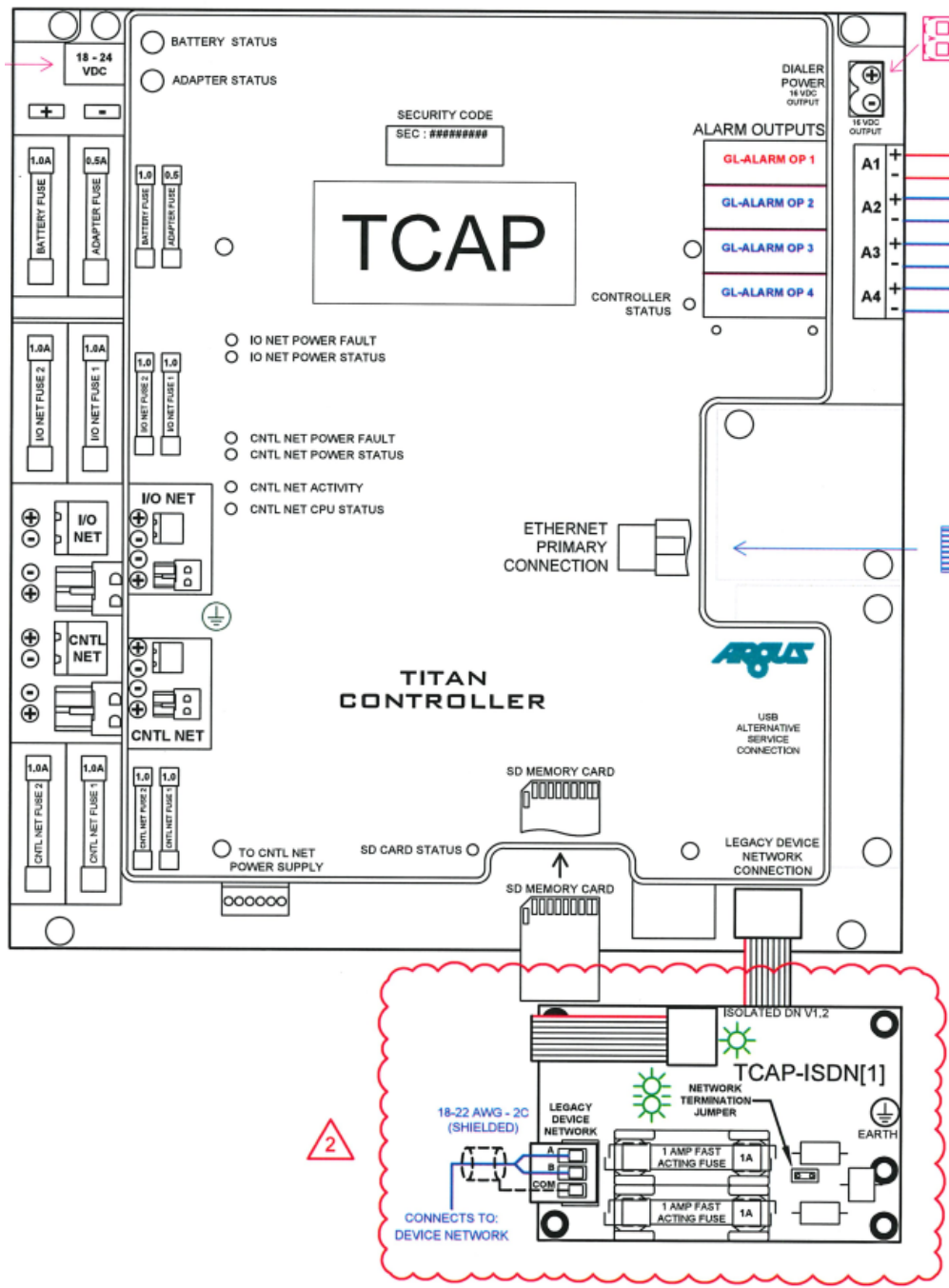


Figure 4.3: Argus Titan Controller and Argus ISODN: Isolated (Optical) Device Network Board circled in red.

can be done natively within the Argus system to offload resources from downstream devices, so it is not necessary for the BBB coordinator to perform the conversions in this application.

4.3 Results

I was able to integrate my custom traditional IoT LoRa-based sensor tag through the Argus Controls system's Modbus interface. This proof-of-concept provided the scaffold for us to develop the VLC system, and gave us confidence in the usability of the system as a drop-in replacement for the costly Argus Omnisensor. Figure 4.4 shows that the traditional IoT system tracks with the Argus Omnisensor, albeit with a slight temperature offset of approximately 1.5 °C. This may be attributed to the placement of the Argus Omnisensor suspended in the center of the greenhouse where the warmer air may be, while the traditional IoT sensor tag was in the corner of the greenhouse on a tabletop, where colder air may settle.

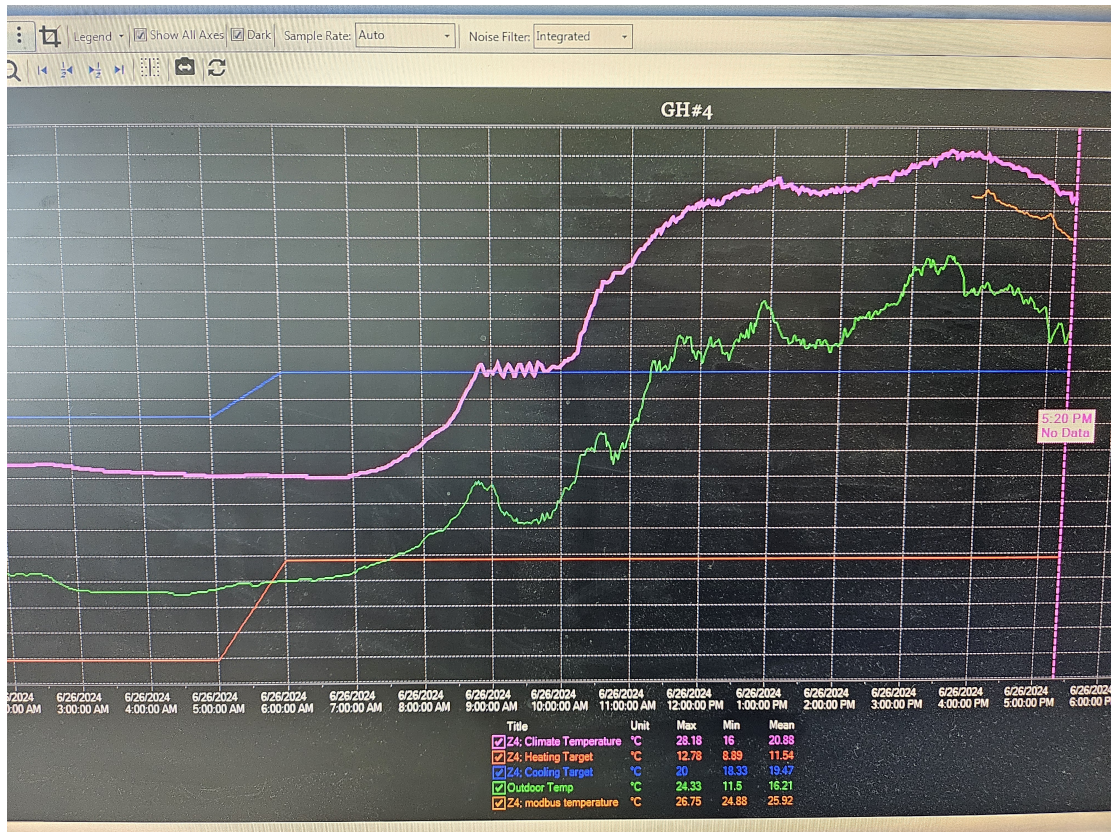


Figure 4.4: Argus Controls environmental status graph of a greenhouse equipped with a traditional IoT sensor that I designed. The short orange (traditional IoT) line below the magenta line (Argus Omnisensor) shows that the temperature tracks the Argus Omnisensor, but may need offset adjustment. (Note: the Omnisensor was suspended approximately 1.5 m above the ground in the center of the greenhouse, while the traditional IoT sensor tag was placed on a bench approximately 1 m above the ground at a corner of the greenhouse. The difference in observed temperature at the two sensor placement areas indicates the necessity for locationally-relevant sensor readings in greenhouses.)

Chapter 5

Discussion and Future Work

Overall, while the performance of the VLC downlink outperformed OOK in BER under indoor conditions, the performance did not fully meet my expectations when under outdoor irradiance conditions. In Figure 3.15, I observed that CSS displayed near-maximal BER above -20 dB regardless of spread factor. While CSS ($SF = 12$) did in fact perform better than OOK between -20 dB and +20 dB, I anticipated strong BER performance even under conditions up to or exceeding -30 dB, which is the approximate signal strength that I anticipated based on daylight noise readings and the luminosity of the XtremeLUX LED transmitters.

There are multiple areas that could be contributing to the perceived poor performance of CSS under sunlight conditions. Firstly, the model may have an incomplete adaptation of the free space path loss formula. The path loss formulas from multiple sources [11] [18] [12] [2] all acknowledge an inverse distance relationship ($\frac{1}{d^2}$), but some models incorporate Lambertian radiation characteristics. A combined path loss model that more completely describes the “antenna” (LEDs and solar panels) gain and di-

rectionality would improve the accuracy of my simulations and system expectations. Secondly, the model also assumes a rather narrow chirp bandwidth between 200 Hz and 2000 Hz. The chirp bandwidth was low to match the frequency characteristics of the solar panel receiver, which faces significant attenuation above a few thousand kHz. As with LoRa, a wider chirp bandwidth helps to facilitate the successful demodulation of chirp symbols since any noise must now be spread across the wider spectrum to impede demodulation. Thirdly, the model borrows as much as possible from LoRa. The parameters for LoRa, such as the spread factor, are tuned and well-suited for the RF medium. However, the ideal parameters for CSS VLC may instead be vastly different from its RF counterpart (and may be extremely hardware-dependent on both the capabilities of the receiver and the transmitter). Lastly, solar panels are not optimized for the high frequency switching that is present in VLC. Typical VLC systems use photodiodes which have less signal attenuation at higher frequencies. A more rigorous evaluation of the solar cells could help to identify the optimal chirp frequencies and symbol period. I believe that these key areas are the most likely contributors to the poor outdoor performance of the FIAT LUX system.

There are multiple areas that are undergoing revisions and improvements. The RF backscatter uplink is under development using universal software radio peripherals (USRP) as the RF backscatter router while the sensors may adapt existing low-power low-bitrate RF backscatter designs such as [43] and [42].

In addition to developing the RF backscatter uplink, the VLC downlink also has room for improvement. The transmission range can be improved by selecting a solar cell configuration that maximizes input swing, and also designing an input stage

with higher gain. The immunity to noise can be further improved by adding a bandpass filter after the comparator, applying an optical coating on the solar panel to reduce or remove the effect of wavelengths outside of the LED transmitter's wavelengths, or by adjusting the VLC link parameters (such as the increasing the chirp bandwidth or increasing the chirp period). In all of the VLC improvements listed above, the major tradeoff is an increased power consumption cost at the wireless sensor tag. Implementing these improvements may require resizing the solar panel area or adding a battery backup to satisfy the increased power draw.

Beyond improving the communications link of the system, integration and community involvement is also an area of future work. To maximize the impact of the VLC platform, adding additional interfaces such as etherCAT or Profinet for connecting with alternative greenhouse/industrial control systems can reduce the effort needed to adopt the system.

The prototype developed in FIAT LUX was a single-user VLC system. For future deployments in large greenhouses, there is room for improvement in developing a medium access control layer to facilitate simultaneous shared use of the visible light medium. Some possibilities include the use of frequency division multiple access techniques to divide chirp frequency bands into distinct channels in a manner similar to WiFi.

Touching upon the analysis discussed in Chapter 5, a more thorough examination of CSS VLC through the lens of information theory (i.e. channel capacity, joules per bit) would be appropriate to develop a more complete simulation model. By deriving the channel characteristics and building a solid mathematical understanding of how

each parameter of the system affects the VLC link, I may be able to determine the ideal parameters most suitable for VLC rather than simply adopting parameters from LoRa.

Chapter 6

Conclusion

In conclusion, my work enabled a visible light communication downlink that is capable of transmitting commands to low-power wireless sensors in greenhouse environments. My work primarily revolved around the development of the embedded Linux systems that support and interface with both ends of the communications link, which includes the sensor manager and the sensor itself. In addition to the design, prototyping, and troubleshooting of the VLC downlink's embedded aspects, I also developed the LoRa-based traditional IoT system which served as the precursor to the VLC system. Throughout the project, I have developed a functioning (albeit short-range) prototype of a VLC link.

While performance of the system did not fully meet expectations in outdoor lighting conditions, I hope that future work can be done to improve VLC development. I anticipate that improvements to CSS VLC will be vital in reducing the energy costs incurred by greenhouse sensor networks.

This thesis presents the development of a visible light communication -based

downlink that permits an ultra-low power wireless sensing solution for protected agriculture applications. As greenhouses increasingly turn to LEDs to overhaul aging and expensive lighting solutions, VLC is poised to adopt a dominant position in the agricultural sensing sector. VLC will not only help to reduce upfront and operational costs for agricultural sensing, but also enable the next generation of smart farming frameworks to obtain plant health data with higher locational precision.

Bibliography

- [1] Fawzia Abdel-Rahman, Bethel Okeremgbo, Fatimah Alhamadah, Sakha Jamadar, Kevin Anthony, and Mahmoud Saleh. Caenorhabditis elegans as a model to study the impact of exposure to light emitting diode (led) domestic lighting. *Journal of environmental science and health. Part A, Toxic/hazardous substances & environmental engineering*, 52:1–7, 01 2017.
- [2] A.G. Al-Ghamdi and J.M.H. Elmirghani. Performance comparison of lsms and conventional diffuse and hybrid optical wireless techniques in a real indoor environment. *IEE Proceedings - Optoelectronics*, 152:230–238, 2005.
- [3] Rens Bloom, Marco Zúñiga Zamalloa, and Chaitra Pai. Luxlink: creating a wireless link from ambient light. In *Proceedings of the 17th Conference on Embedded Networked Sensor Systems*, SenSys '19, page 166–178, New York, NY, USA, 2019. Association for Computing Machinery.
- [4] Rens Bloom, Marco Zúñiga Zamalloa, and Chaitra Pai. Luxlink: creating a wireless link from ambient light. In *Proceedings of the 17th Conference on Embedded Networked Sensor Systems*, SenSys '19, page 166–178, New York, NY, USA, 2019. Association for Computing Machinery.

- [5] Kyle Booth, Jasmine Shepard, Remy Hutheesing, and Joe Sullivan. Controlled environment horticulture. *California Codes and Standards Enhancement (CASE) Program*, 2025.
- [6] Texas Instruments. CC1125 datasheet. url: <https://www.ti.com/product/CC1125>.
- [7] Land Processes Distributed Active Archive Center. *Workflow Examples - Vegetation*. Sioux Falls, South Dakota, 2018. Table 43. Irrigation for Nursery, Greenhouse, and Other Horticultural Crops Grown Under Protection: 2018 and 2013.
- [8] Chun-Ling Chan, Hsin-Mu Tsai, and Kate Ching-Ju Lin. Poli: Long-range visible light communications using polarized light intensity modulation. In *Proceedings of the 15th Annual International Conference on Mobile Systems, Applications, and Services*, MobiSys '17, page 109–120, New York, NY, USA, 2017. Association for Computing Machinery.
- [9] Argus Controls. Isolated device network board datasheet ttn-isodn. url: <https://arguscontrols.com/uploads/documents/TTN-ISODN-1.2-Data-Sheet-Rev.-July-2017.pdf>.
- [10] Vitor Fialho and Fernando Azevedo. Wireless communication based on chirp signals for lora iot devices. *i-ETC : ISEL Academic Journal of Electronics Telecommunications and Computers*, 4(1):6, 2018.
- [11] H.T. Friis. A note on a simple transmission formula. *Proceedings of the IRE*, 34(5):254–256, May 1946.

- [12] F.R. Gfeller and U. Bapst. Wireless in-house data communication via diffuse infrared radiation. *Proceedings of the IEEE*, 67(11):1474–1486, Nov 1979.
- [13] Seyed Keyarash Ghiasi, Marco A. Zúñiga Zamalloa, and Koen Langendoen. A principled design for passive light communication. In *Proceedings of the 27th Annual International Conference on Mobile Computing and Networking, MobiCom '21*, page 121–133, New York, NY, USA, 2021. Association for Computing Machinery.
- [14] Climapod, url: <https://climapod.com/the-history-of-greenhouses/>.
- [15] Grow Lights Australia. What is a Par map?. url: <https://growlightsaustralia.com/what-is-a-par-map/>.
- [16] Borja Genoves Guzman, Muhammad Sarmad Mir, Dayrene Frometa Fonseca, Ander Galisteo, Qing Wang, and Domenico Giustiniano. Prototyping visible light communication for the internet of things using openvlc. *IEEE Communications Magazine*, 61(5):122–128, May 2023.
- [17] Harald Haas, Liang Yin, Yunlu Wang, and Cheng Chen. What is lifi? *J. Lightwave Technol.*, 34(6):1533–1544, Mar 2016.
- [18] Babar Hussain, Fengyu Che, C. Patrick Yue, and Liang Wu. Link budget analysis for visible light communication systems. In *2015 IEEE International Wireless Symposium (IWS 2015)*, pages 1–4, March 2015.
- [19] Jin-Shyan Lee, Yu-Wei Su, and Chung-Chou Shen. A comparative study of wireless protocols: Bluetooth, uwb, zigbee, and wi-fi. In *IECON 2007 - 33rd Annual Conference of the IEEE Industrial Electronics Society*, pages 46–51, Nov 2007.

- [20] Jiangtao Li, Angli Liu, Guobin Shen, Liqun Li, Chao Sun, and Feng Zhao. Retro-vc: Enabling battery-free duplex visible light communication for mobile and iot applications. In *Proceedings of the 16th International Workshop on Mobile Computing Systems and Applications*, HotMobile '15, page 21–26, New York, NY, USA, 2015. Association for Computing Machinery.
- [21] Eric B. LoRa Documentation - RSSI. url: <https://lora.readthedocs.io/en/latest/#rssi>.
- [22] Luiz Eduardo Mendes Matheus, Alex Borges Vieira, Luiz F. M. Vieira, Marcos A. M. Vieira, and Omprakash Gnawali. Visible light communication: Concepts, applications and challenges. *IEEE Communications Surveys & Tutorials*, 21(4):3204–3237, Fourthquarter 2019.
- [23] Kais Mekki, Eddy Bajic, Frederic Chaxel, and Fernand Meyer. Overview of cellular lpwan technologies for iot deployment: Sigfox, lorawan, and nb-iot. In *2018 IEEE International Conference on Pervasive Computing and Communications Workshops (PerCom Workshops)*, pages 197–202, March 2018.
- [24] Muhammad Sarmad Mir, Borja Genoves Guzman, Ambuj Varshney, and Domenico Giustiniano. Passivelifi: rethinking lifi for low-power and long range rf backscatter. In *Proceedings of the 27th Annual International Conference on Mobile Computing and Networking*, MobiCom '21, page 697–709, New York, NY, USA, 2021. Association for Computing Machinery.
- [25] Mrinmoyee Mukherjee. Visible light communication-a survey of potential research

- challenges and advancements. In *2017 Second International Conference on Electrical, Computer and Communication Technologies (ICECCT)*, pages 1–8, Feb 2017.
- [26] Maria Rita Palattella, Mischa Dohler, Alfredo Grieco, Gianluca Rizzo, Johan Torsner, Thomas Engel, and Latif Ladid. Internet of things in the 5g era: Enablers, architecture, and business models. *IEEE Journal on Selected Areas in Communications*, 34(3):510–527, March 2016.
- [27] ParSource. G11h and glx55031 datasheets. ParSource GL1H and GLX55031 datasheets not available online.
- [28] C. B. Honsberg and S. G. Bowden, “Quantum Efficiency,” page on www.pveducation.org, 2019.
- [29] Brecht Reynders and Sofie Pollin. Chirp spread spectrum as a modulation technique for long range communication. In *2016 Symposium on Communications and Vehicular Technologies (SCVT)*, pages 1–5, Nov 2016.
- [30] K. Sindhubala and B. Vijayalakshmi. Design and performance analysis of visible light communication system through simulation. In *2015 International Conference on Computing and Communications Technologies (ICCCT)*, pages 215–220, Feb 2015.
- [31] Prabhakar T, Vishwas Shashidhar, G S Aishwarya Meghana, R. Venkatesha Prasad, and Garani Vittal Pranavendra. Zero energy visible light communication receiver for embedded applications. *SIGBED Rev.*, 15(2):37–43, June 2018.

- [32] United Sci Handheld Digital Luxmeter. url: <https://www.unitedsci.com/digital-luxmeter.html>.
- [33] National Agricultural Statistics Service U.S. Department of Agriculture. *2018 Irrigation and Water Management Survey*. USDA, USDA-NASS, 1400 Independence Ave., SW Washington, DC 20250, 2018. Table 43. Irrigation for Nursery, Greenhouse, and Other Horticultural Crops Grown Under Protection: 2018 and 2013.
- [34] National Agricultural Statistics Service U.S. Department of Agriculture. *2022 Census Full Report*. USDA, USDA-NASS, 1400 Independence Ave., SW Washington, DC 20250, 2022. Table 39. Floriculture and Bedding Crops, Nursery Crops, Propagative Materials Sold, Sod, Food Crops Grown Under Glass or Other Protection, and Mushroom Crops: 2022 and 2017.
- [35] National Agricultural Statistics Service U.S. Department of Agriculture. *2023 Irrigation and Water Management Survey*. USDA, USDA-NASS, 1400 Independence Ave., SW Washington, DC 20250, 2023. Table 46. Irrigation for Nursery, Greenhouse, and Other Horticultural Crops Grown Under Protection: 2023 and 2018.
- [36] Lorenzo Vangelista. Frequency shift chirp modulation: The lora modulation. *IEEE Signal Processing Letters*, 24(12):1818–1821, Dec 2017.
- [37] Lorenzo Vangelista. Frequency shift chirp modulation: The lora modulation. *IEEE Signal Processing Letters*, 24(12):1818–1821, 2017.
- [38] Lucas Vanhaelewyn, Dominique Van Der Straeten, Barbara De Coninck, and

- Filip Vandenbussche. Ultraviolet radiation from a plant perspective: The plant-microorganism context. *Frontiers in Plant Science*, 11, 2020.
- [39] Jia Wang, Ahmed Al-Kinani, Jian Sun, Wensheng Zhang, and Cheng-Xiang Wang. A path loss channel model for visible light communications in underground mines. In *2017 IEEE/CIC International Conference on Communications in China (ICCC)*, pages 1–5, Oct 2017.
- [40] Qing Wang, Danilo De Donno, and Domenico Giustiniano. Research platform for visible light communication and sensing systems: demonstration abstract. In *Proceedings of the 15th International Conference on Information Processing in Sensor Networks, IPSN '16*. IEEE Press, 2016.
- [41] XtremeLUX. Lf11 datasheet. XtremeLUX LF11 datasheet is not publicly released.
- [42] Pengyu Zhang, Dinesh Bharadia, Kiran Joshi, and Sachin Katti. Hitchhike: Practical backscatter using commodity wifi. In *Proceedings of the 14th ACM Conference on Embedded Network Sensor Systems CD-ROM, SenSys '16*, page 259–271, New York, NY, USA, 2016. Association for Computing Machinery.
- [43] Pengyu Zhang, Colleen Josephson, Dinesh Bharadia, and Sachin Katti. Freerider: Backscatter communication using commodity radios. In *Proceedings of the 13th International Conference on Emerging Networking EXperiments and Technologies, CoNEXT '17*, page 389–401, New York, NY, USA, 2017. Association for Computing Machinery.